Heritage Science

RESEARCH

Open Access

Virtual reconstruction of the painting process and original colors of a color-changed Northern Wei Dynasty mural in Cave 254 of the Mogao Grottoes

Chai Bolong[1,2,3,4], Yu Zongren[4], Sun Manli[1,2,3], Shan Zhongwei[4], Zhao Jinli[4], Shui Biwen[4], Wang Zhuo[4], Yin Yaopeng[4] and Su Bomin[4*]

Abstract

The Northern Wei Dynasty (386–534 CE) murals of Cave 254 in the Mogao Grottoes, China, have been extensively affected by pigment color changes and fading. These issues severely hinder efforts to correctly understand the value and painting process of murals from this historic period. The virtual reconstruction of the faded murals reflects the analysis results of the pigments applied during the painting process and provides a new direction for conservation and art research. However, simple virtual reconstructions may not be accurate owing to deficiencies in our understanding of the color-changed pigments and fading of image lines. In this study, multi-band imaging (MSI) was performed to obtain infrared-reflected false color, ultraviolet-reflected false color, and ultraviolet luminescence images of the mural. A portable X-ray fluorescence spectrometer, portable digital microscope, scanning electron microscope, energy dispersive X-ray spectrometer, liquid chromatography–mass spectrometer, and confocal Raman microscope were used. Non-invasive and minimally invasive analyses of local portions of different color areas were performed to identify their pigments and map the strata, and a hue–saturation–brightness palette was constructed for these pigments. Finally, the pigment analysis results were combined with the multi-band image features to determine the pigment distribution of the mural, which was then used to virtually reconstruct the original color and appearance of the faded mural under ideal conditions. This study is the first to use a virtual reconstruction based on objective analyses to simulate the original color, painting processes, and pigment stratigraphy of a mural from the Northern Wei Dynasty. A preliminary discussion of the relationship between the painting processes of the mural and color changes in its pigments was also performed. The findings of this study will provide new perspectives on the study of Northern Wei Dynasty murals.

Keywords: Virtual reconstruction, Multi-band imaging, Pigment analysis

Introduction

The Mogao Grottoes is located 25 km southeast of Dunhuang city, Gansu Province, China. It is a cave system containing 735 caves, 492 of which contain polychromatic sculptures and murals. The oldest caves in this system were constructed in 366 CE, during the former Qin Dynasty. The construction of these caves continued for over 1600 years, until the end of the Yuan Dynasty (1271–1368 CE). As a whole, the Mogao Grottoes

*Correspondence: SuBomin_dha@126.com

[4] National Research Center for Conservation of Ancient Wall Paintings and Earthen Sites, Gansu Province, Dunhuang Academy, Dunhuang 736200, China

Full list of author information is available at the end of the article

Springer Open

© The Author(s) 2022. **Open Access** This article is licensed under a Creative Commons Attribution 4.0 International License, which permits use, sharing, adaptation, distribution and reproduction in any medium or format, as long as you give appropriate credit to the original author(s) and the source, provide a link to the Creative Commons licence, and indicate if changes were made. The images or other third party material in this article are included in the article's Creative Commons licence, unless indicated otherwise in a credit line to the material. If material is not included in the article's Creative Commons licence and your intended use is not permitted by statutory regulation or exceeds the permitted use, you will need to obtain permission directly from the copyright holder. To view a copy of this licence, visit http://creativecommons.org/licenses/by/4.0/. The Creative Commons Public Domain Dedication waiver (http://creativecommons.org/publicdomain/zero/1.0/) applies to the data made available in this article, unless otherwise stated in a credit line to the data.

contain 45,000 m^2 of murals and over 2000 polychromatic sculptures, which contain information on the livelihoods, cultures, religions, and arts of 10 different dynasties, thereby rendering it one of the most important grottos in the world. In 1987, the United Nations Educational, Scientific, and Cultural Organization (UNESCO) introduced the Mogao Grottoes into the UNESCO World Heritage List. The murals in Cave 254, which was dug during the Northern Wei Dynasty, are representative of Mogao Grotto art from this period. The Buddhist mural (i.e., pictures representing a story from Buddhist scripture) on the southern wall of this cave is "Prince Sattva Sacrifices Himself to the Starving Tigress" (hereafter referred to as "Prince Sattva"), one of best-known stories in Buddhist mythology. Because this mural combines Indian and West Asian Buddhism with the traditional Chinese style, it is immensely valuable for studies on the propagation of Buddhist art in China and its integration with local Chinese art. Furthermore, detailed studies on this mural could improve methods to preserve and repair murals from this period. The Prince Sattva mural measures 168 cm wide and 150 cm tall, and it narrates a story from a past life of the Buddha using a series of pictures within a rectangular space. Each picture represents an event that occurred at a different time and place. This approach overcomes the limitations of 2D art in its ability to describe the passage of time, and the mural is a classic example of the narrative illustrations that emerged after the Han dynasty (202 BCE–220 CE). The story told by this mural consists of five scenes: (1) Prince Sattva vows to save the tigress; (2) the prince pierces his neck and dives from the cliff; (3) the tigress feeds herself on Sattva's body; (4) Sattva's family mourns his death, and (5) Apsarases (a celestial being in Indian mythology) floats around a pagoda holding Sattva's bones (Fig. 1). Owing to the importance of this particular mural in the history of the Mogao murals, many artists and conservationists have shown great interest in the pigments, colors, and painting processes used in this mural, as well as its artistic value [1–4]. Many have attempted to reimagine the original color and appearance of this mural, and, to this end, a variety of methods have been used to reconstruct the mural.

In the past, the main purpose of mural reconstruction research was to study fine art and obtain a virtual presentation of restoration effects. Research in this field usually takes on the forms of art replication and virtual reconstruction [5]. Art replication is performed by experienced artists, and it is a subjective process based on comparisons with well-preserved murals that are contemporary to the degraded, to-be-replicated mural. An example of a replication being used to reconstruct a mural is the "Donor portrait of Lady Wang from Taiyuan in worship" from Cave 130, which was replicated by Duan Wenjie [6]. Virtual reconstruction, an approach that is currently in vogue, refers to the use of computational image processing algorithms, such as image segmentation, texture synthesis, machine learning, and neural networks, to digitally reconstruct the color and details of an artistic product [7–12]. These methods could inform and pave the way for future attempts to recreate the original appearance of ancient murals. Unfortunately, such techniques may be inapplicable to murals with changed colors owing to gaps in our knowledge of the faded image and its color-changed pigments. The accuracy of digital replicas or reconstructions based on machine learning can also be affected by the conditions of the working space, the quality of the image pixels, and the accuracy of the pigment-color analysis. Furthermore, machine learning methods require massive amounts of data, and constructing the large number of sample models required by these methods within a short time is difficult. This limitation could ultimately reduce the accuracy of color classification and reconstruction by machine learning methods.

Mogao murals are well known to have a preparatory layer consisting of coarse (sand and wheat-straw) and fine (sand + bast and leaf fiber) soil, which is covered by preparatory and pigment layers. Repeated studies by scholars and research institutes in China and beyond have confirmed that the colors used in the Mogao murals primarily consist of red, blue, green, white, and black, which come from over 20 natural mineral pigments. Some murals even use organic dyes, such as indigo, lac, and madder [13–18]. The environmental factors and complexity of the pigments and painting techniques render these murals susceptible to pigment degradation, which leads to color changes. For instance, pigments containing Hg, Pb, and As are easily degraded by photochemical reactions, air pollution, microbial action, or other complex chemical reactions, which could change their color and appearance [19–24]. Organic pigments are also susceptible to photochemical or microbial degradation [25]; thus, assessing whether organic pigments were applied to a mural using visible light alone is difficult. Mogao murals are extensively affected by these chemical changes, and accurately ascertaining the original colors of the faded murals and objectively performing virtual reconstructions of these murals are challenging.

In this work, we created a digital representation of the Prince Sattva mural based on an extensive investigation and analysis of its color pigments. Compared with previous forms of mural reconstruction, digital reconstruction (for mural preservation and artistic research) enables the final visualization of extensive studies and provides a deeper understanding of the simulation and analyses of the pigment usage rules and painting

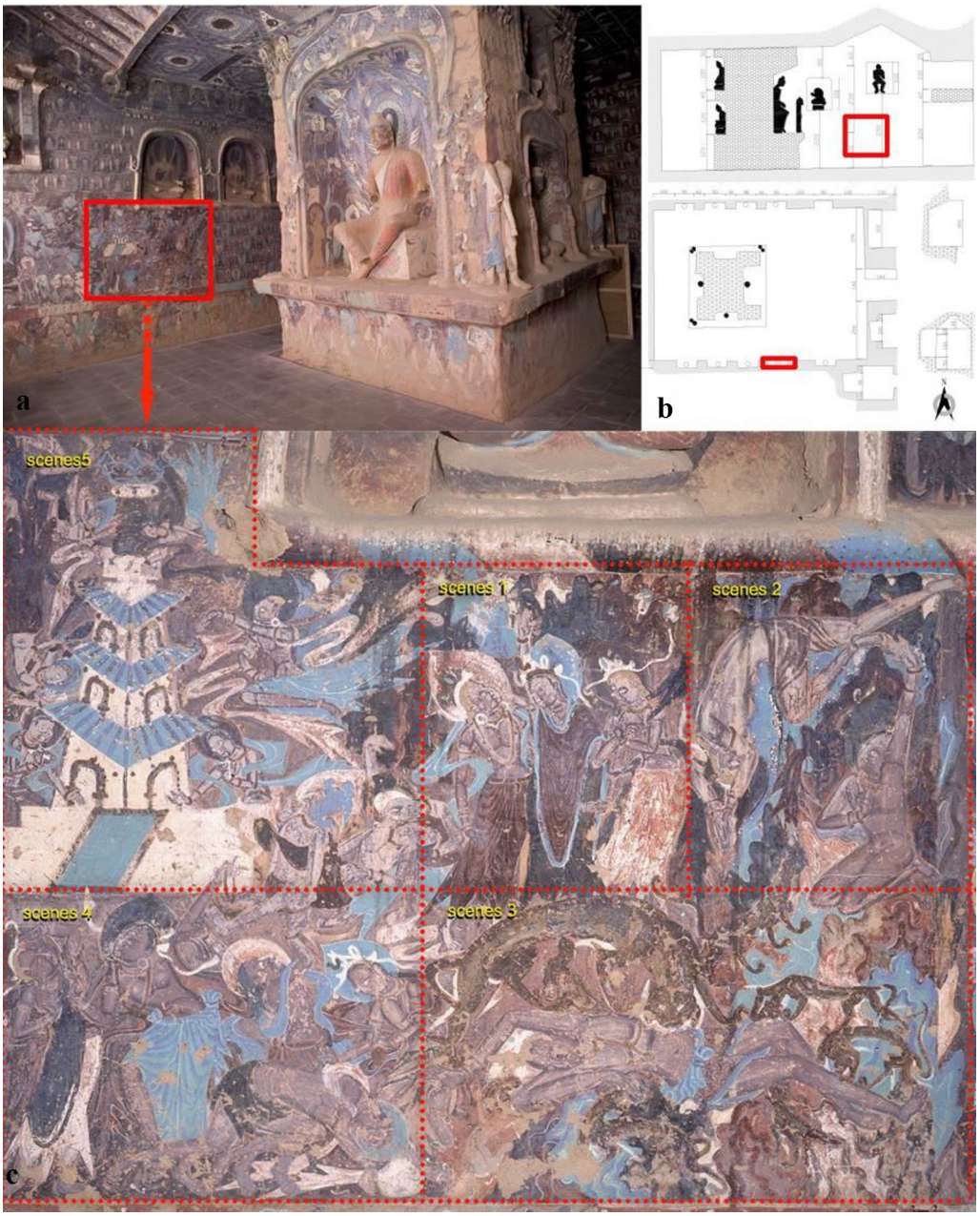

Fig. 1 The current condition of the "Prince Sattva" mural on the south wall of Cave 254: **a** Cave section and floor plan, **b** cave scene, and **c** Prince Sattva

procedures of Northern Wei Dynasty murals. The results of our efforts to restore the colors of the original mural and faded details of the images can be used as a visual aid to support pigment analysis and process understanding. As the pigment analysis method used in this work is undoubtedly the pillar technology of cultural relic protection, our comprehensive analysis results could serve as an important basis for improving the objectivity and feasibility of the virtual reconstruction of discolored and faded murals. Moreover, our findings present a new perspective for the analysis and display of murals in the Mogao Grottoes.

Methodology and equipment

Methodology

The processes of virtual reconstruction can be broadly divided into two parts: a preliminary investigation and digital painting restoration. The first part involves the extraction of information from the faded image and the study of pigment types, both of which are necessary for objective and realistic virtual reconstructions. The study of faded and color-changed pigments is the primary focus and challenge of this work.

First, ultraviolet-induced visible luminescence (UVL) and IR photography were used to detect organic dyes and degraded details that are invisible to the naked eye. Infrared-reflected false-color (IRRFC) and UV-reflected false-color (UVRFC) images were then used to determine the areas that were painted with each type of pigment as pigments of the same type will have similar false-colors in IRRFC and UVRFC images. However, as the mural contains complex mixtures and layers of color and is affected by color changes, identifying pigments based on the multi-band images of standard pigment samples is not a straightforward task. In other words, the IRRFC and UVRFC characteristics of the mural may not perfectly match those of the multi-band reference. Therefore, as an auxiliary investigation method, the identification ability of multi-band imaging (MSI) is limited by the mural painting technology, the preservation of mural pigments, and its own application methods. Nonetheless, because pigments of the same type will exhibit similarities in certain spectral bands, IRRFC and UVRFC images could be used to preliminarily determine the distribution of unidentified pigments in the mural. The exact identification of pigments and color-changed compounds can only be achieved using noninvasive and/or minimally invasive analytical methods when conditions permit.

Next, non-invasive and/or minimally invasive analytical methods were applied to analyze the relationship between pigment type and color in each color area of the mural and assess the effects of paint layering on the surface color. Because minimizing damage to the mural is necessary, only trace samples were obtained from the damaged edges of the pigment layers in different color areas. The samples were divided into powder and block, and each sample was controlled within 0.2 g for spectral analysis and cross-sectional observation. Finally, the distribution of each pigment in the mural was determined by the combining the analysis results of different instruments and the color region division results of the false-color images (IRRFC and UVRFC).

The types of pigments used in the mural were determined via the pigment analysis process. A multi-band reference file was also used to identify the corresponding pigment samples for comparison. Color saturation and brightness (HSB color model) values were extracted from the VISR images of each pigment sample, and these HSB values were used to construct a digital palette. Finally, the virtual reproduction of the mural was achieved by examining the multi-band image display details of its lines and the paint distribution data on the mural for digital coloring.

Equipment

A modified Nikon D7000 camera with a maximum resolution of 4928 px × 3264 px (16.2 MP) was used for technical photography (UV–VIS-IR). The spectral response of this camera's sensor was expanded to approximately 300–1000 nm by removing its built-in IR filter [26–28]. A 35 mm f2.8 DX lens was installed on the camera, and the spectral bandwidth of the camera was limited using various filters. A pair of Godox AD360 halogen flashes [360 W, 5,600 ± 200 K, 80 (M ISO 100), 1/10,000–1/300 S] were used as light sources. These flashes were modified by replacing their plastic filters with a variety of filters depending on the desired spectral bandwidth. The use of bandpass filters on the light source and receiver (camera lens) has been proven to be a reliable method to obtain multi-band images because it eliminates the need for different light sources for each spectral band and reduces the need for total darkness during image acquisition (especially photoluminescence images). Professor Giovanni Verri has contributed tremendously to the development of this approach [29]. The bandwidths of the filter sets used in this study are shown in Table 1.

Besides the camera, light source, and filters, the X-rite Color Checker and Spectralon® reflectance standards are also important accessories for technical photography as they are used for color correction and diffuse reflection spectroscopy. All multi-band images were taken in manual mode. The parameters of the VISR and IRR images were F8, 1/200 S, and ISO: 100. The parameters of the UVR images were F2.8, 1/200 S, and ISO: 100. The parameters of the UVL images were F2.8, 1/200 S, and ISO: 400. The two light sources were oriented symmetrically about the focal axis of the camera at an angle of 45°, and the power of the flashes was adjusted according to the straight-line distance between the lens and mural. Post-processing of the spectral images and generation of false-color images were performed using Photoshop and Nip2 and BM-workspace [30–35]. The postprocessing procedures, workflows, and data requirements are detailed in Refs. [36].

Multi-band image reference file for pigments

The multi-band reference file is a collection of multi-band digital image files that is used to identify the pigment of the study object. These files were from multi-band

Table 1 Incoming and outgoing filter sets used for reflectance and luminescence imaging

Method	Flash filters (77 mm)	Excitation band range	Lens filters (52 mm)	Emission band range
VISR	Plastic diffuser	185–2000 nm	IDAS (360–700 nm) + KV418 (cut-on above 400 nm)	400–700 nm
IRR	——	185–2000 nm	Schott RG715/830/1,000 (cut-on above 715/830/1000 nm)	715–1000 nm
UVR	XNiteCC1 (330–700 nm) + XNite330C (200–400 nm)	330–400 nm	XNiteCC1 (330–700 nm) + XNite330C Shortpass (200–400 nm)	330–400 nm
UVL	XNiteCC1 (330–700 nm) + XNite330C (200–400 nm)	330–400 nm	IDAS (360–700 nm) + KV418 (cut-on above 400 nm)	400–700 nm

VISR = visible light reflectance; IRR = infrared reflectance; UVR = ultraviolet reflectance; UVL = ultraviolet-induced luminous. Filter source: https://maxmax.com/. The plastic diffuser does not block ultraviolet light

(360-1000 nm) images of pigment samples, and samples were pigments mixed with gelatin at a ratio of 3–5% [13]. The photographic parameters and postprocessing procedures were analogous to the process of collecting multi-band images of the research subject. By comparing the spectral reflectance and luminescence characteristics of the studied objects with multi-band image reference files, some single-layer pigments can be preliminarily identified. The advantage of this method is that it is simple and intuitive, while the disadvantage is that the ability to identify pigments will be limited by mural preservation conditions and paint changes. As an auxiliary method of nondestructive analysis, this method has been applied to the investigation of pigments in painted cultural relics by some scholars [37–39]. However, the Mogao Grottoes murals were painted mainly with mineral pigments, and the paint samples used in the multi-band image reference files were obtained from various modern manufacturers and not by the murals themselves. The first step is to ensure a qualitative analysis of the material composition and structure of these paint samples. The pigment samples were subjected to X-ray diffraction (XRD) analysis, to be suitable for purity purposes. We previously performed an experimental study on multi-band references for the pigments used in Mogao murals (Additional file 1: 1.1–1.2). In this study, the reference files were used to assess the chroma and hue of the pigments prior to their color change by extracting the HSB values of the target pigment from the VISR image in its multi-band reference files. The HSB values were utilized to create a digital color palette, which was used to color the virtually reconstructed mural.

Portable X-ray fluorescence (pXRF) analyzer

The pXRF instrument used in this study was a Thermo Fisher Scientific (USA) Niton XL3t 800, which employs an Ag target as its excitation source. The parameters of the pXRF were as follows: tube voltage: 6–50 kV, tube current: 0–200 μA, power: ≤ 2 W, detector: Si-PIN (Si semiconductor detector), resolution: < 190 eV, detection time: 60 s, diameter of analyzed area: 8 mm.

X-ray diffractometer

A DMAX/2500 X-ray diffractometer was used to perform the XRD analysis. The measurements were performed in continuous-scan mode over the 2θ range of 5°–70° with a tube voltage of 40 kV and tube current of 100 mA. Mixed layers from the pigment layer were used as samples, and each sample weighed approximately 0.2 g.

Scanning electron microscopy and energy dispersive X-ray spectroscopy (SEM–EDS)

SEM–EDS spectroscopy was performed using a JSM-6610LV scanning electron microscope (JEOL Ltd., Japan). The analysis was performed with an acceleration voltage of 25 kV, resolution of 5.0 nm, and magnification of 5 × –30,000 × in vacuum mode. A polarized microscope was used to observe 0.2 mg pigment samples and select cross-sections of interest. The samples were embedded in epoxy, polished, platinized, and then placed in the sample chamber of the SEM for cross-sectional analysis.

Liquid chromatograph-mass spectrometer (LC/MS)

Pigment samples were extracted with 0.5 ml methanol for 10 min in a 40 °C bath with ultrasonic irradiation, and then the sample was separated on a Vauquish Flex ultrahigh-performance liquid chromatograph equipped with a vacuum degasser, automatic sampler, column oven and binary pump (Thermo Fisher Scientific, Germany). Mobile phase A was composed of H_2O with 0.1% formic acid, and mobile phase B was composed of 100% acetonitrile. Exactly 5 μL of the samples was injected into a Hypersil Gold C18 column (2.1 mm × 100 mm, 1.9 μm, Thermo Fisher Scientific) and separated at a flow rate of 0.3 mL/min. Gradient elution was performed as follows: 0–12 min, 20% B to 98% B; hold for 5 min; 17.1 min, return 20% B; and re-equilibrate for 3 min. The total run time was 20 min. A Q Exactive high-resolution mass

spectrometer equipped with an electrospray ionization (ESI) ion source was connected to the UHPLC system. The temperatures of the auxiliary gas, ion source, and capillary were set to 300, 450, and 275 °C, respectively, and the flow rates of the sheath and auxiliary gases were set to 6 and 10 L/min, respectively. The stepped collision energies were set to 20, 40, and 60 eV. The spray voltage was set to 3.50 kV for positive- and negative-ion modes. The samples were detected in full-scan MS/dd MS2 acquisition mode with a scan range of 100–1000 m/z at mass resolutions of 70,000 FWHM for MS and 17,500 FWHM for MS/MS. The analytical data were obtained in negative-ion mode.

Portable digital microscope (pDM)

A VH-Z20R (20 × –200 ×) lens and Keyence VHX-600E digital microscope (a built-in illuminator) were used for visible-light microscopy.

Confocal Raman microscope

A LabRAM XploRA (Horiba, France) confocal Raman microscope (m-RS) was used for micro-scale product identification and chemical imaging. This instrument includes a high-stability research-grade microscope with reflective and transmissive Köhler illumination and is equipped with 10 ×, 100 ×, and long working distance 50 × objectives. The instrument also includes high-stability 532 and 785 nm fixed lasers (and their filters) and a computer-controlled multilevel laser attenuator. The microscope is fully confocal; when equipped with 100 × objectives, its spatial resolution is < 1 μm in the XY direction and < 2 μm in the Z direction. The system is equipped with four gratings (2400 gr/mm, 1800 gr/mm, 1200 gr/mm, and 600 gr/mm) and has a spectral resolution of ≤ 2 cm^{-1}. Its spectral repeatability is greater than ± 0.2 cm^{-1}. Two excitation wavelengths, specifically, 532 and 785 nm, were simultaneously used in this experiment; of these, the 532 nm excitation wavelength has higher excitation efficiency and a stronger fluorescence background. By contrast, the 785 nm excitation wavelength has a weaker fluorescence background. The range of Raman frequency shift measured is 100–3000 cm^{-1}.

Digital restoration tools

The digital restoration ware performed using Adobe Photoshop, the Procreate raster graphics editor app, and a Wacom Intuos Pro PTH660 tablet.

Results and discussion

Investigation of image details

Multi-band images can reveal many details that are invisible to the naked eye. In Scene 2, the 830 nm IR image revealed traces of a mesh pattern on the Prince's hair bun (Fig. 2a). After investigation, we found that the traces resemble the contour of the crown of the 'Contemplative Bodhisattva' statue (2nd year of the Eastern Wei Dynasty, 540 CE), which was unearthed in 1954 at the site of the Xiude Temple in Quyang County, Hebei Province. The crown is shaped like an inverted trapezoidal crown with floating cloth pieces attached to it. The Eastern Wei Dynasty (534–550 C.E.) was founded as a result of the disintegration of the Northern Wei; its art forms relate to the cultural legacy of its predecessor (Additional file 1). Although no evidence that these remaining traces are part of the crown has been reported, this finding is rarely found in Mogao Grottoes for a "Prince Sattva" of the same type.

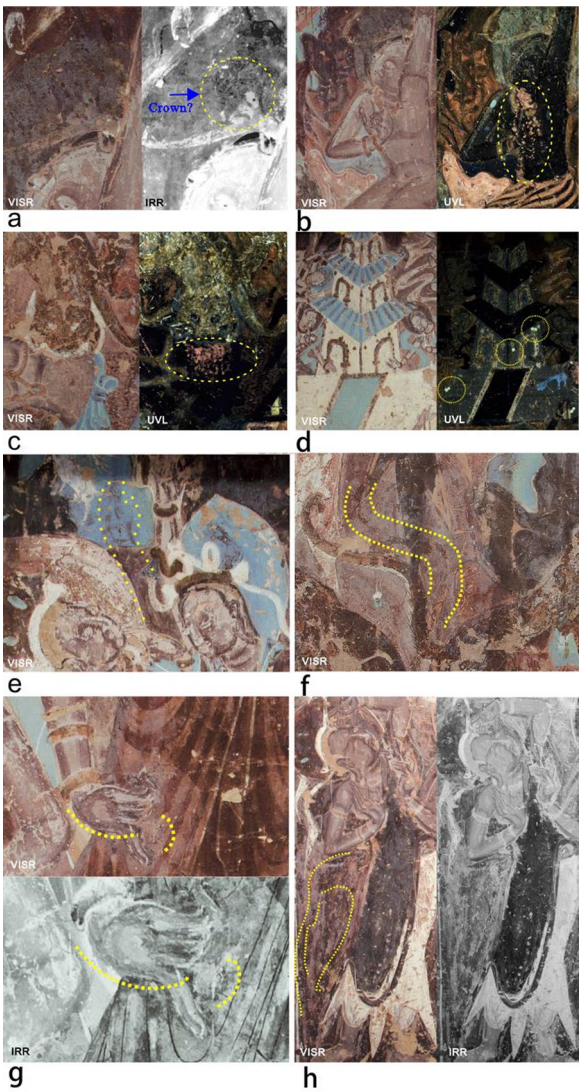

Fig. 2 Multi-band investigation of the mural details

The UVL images revealed scenes that are invisible to the naked eye, such as blood spurting out of the prince's throat when he commits suicide in Scene 2 (Fig. 2b) and coming out of the tigers' mouths when they bite into the prince's body in Scene 3 (Fig. 2c). Neatly arranged circular luminescent dots in Scenes 2 (the Prince's suicide) and 5 (around the pagoda) also caught our attention (Fig. 2d). Based on the appearance of the scene, we speculate that these dots either have some special meaning or are the mistakes and spilled paint residues of the artist.

The multi-band image also shows the artist's modifications to the murals, some of which are enhanced in the IR image. Scene 1 shows two modifications: the raised hand of the prince was moved rightward (Fig. 2e), and the finger of the prince's younger brother (to his right) was changed from curled to outstretched, a trace that is enhanced in the IR image (Fig. 2g). In Scene 3, the tail of a tiger cub was changed from straight to sloping downward (Fig. 2f). In Scene 4, a faint outline of the Bodhisattva robe is seen on the left side after IR image enhancement. Moreover, his waist and legs were moved to the right and drawn to curve toward this direction (Fig. 2h).

Pigment analysis

Overall, the VISR (Fig. 3), IRRFC (Fig. 4), UVRFC (Fig. 5), and UVL (Fig. 6) images clearly revealed the different color areas of the mural. The VISR images showed that the mural currently has 10 color systems, including

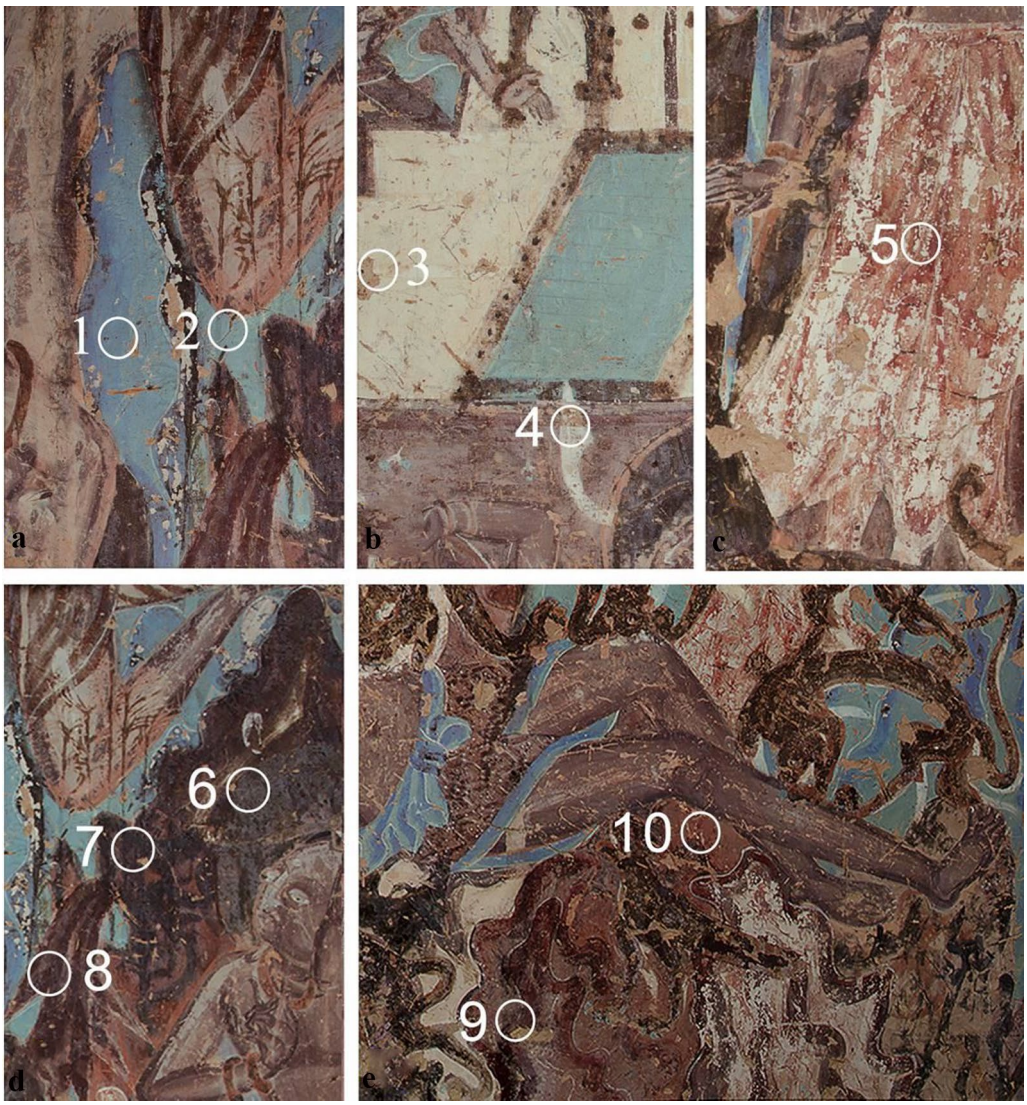

Fig. 3 Partial-view VISR imaging of the Prince Sattva mural and 10 analysis points

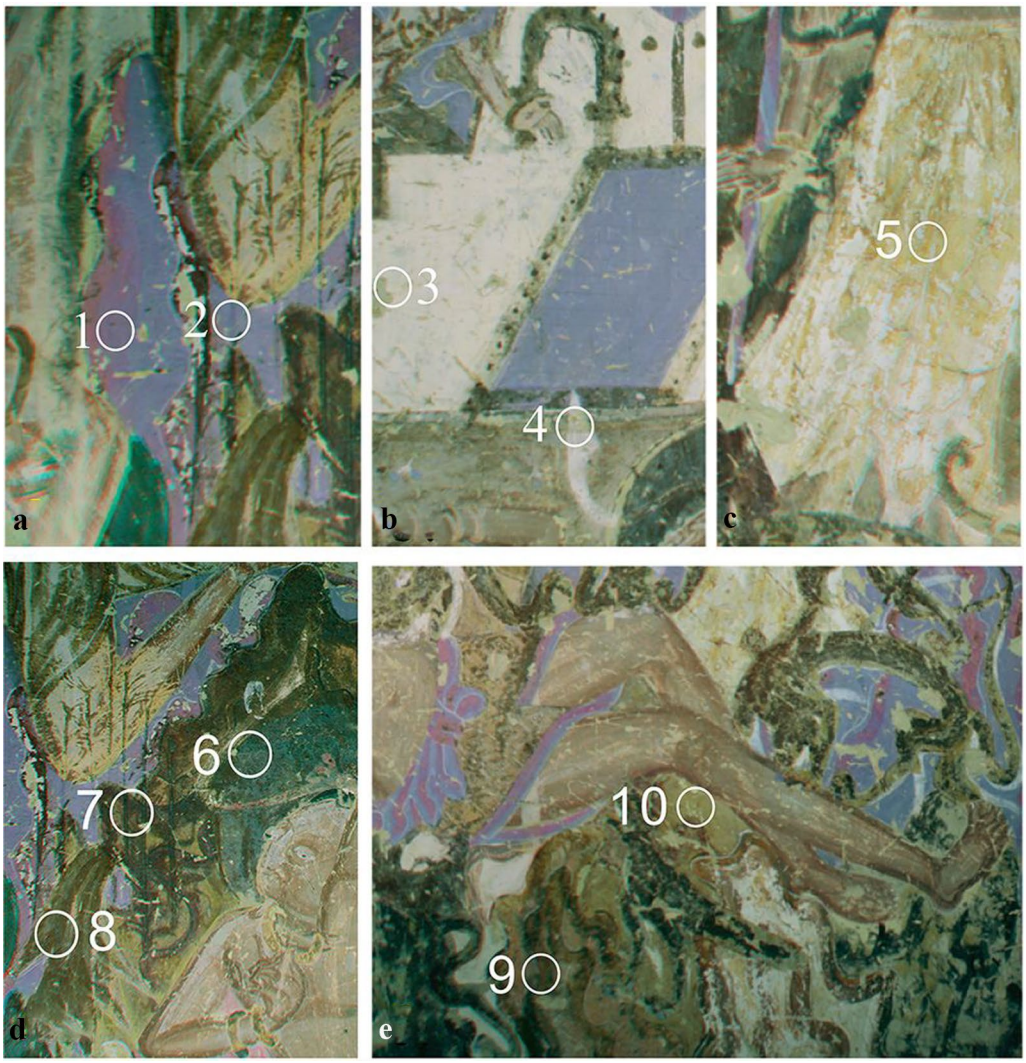

Fig. 4 Partial-view IRRFC imaging of the Prince Sattva mural and 10 analysis points

blue (1), bean green (2), ivory white (3), pure white (4), light red (5), charcoal gray (6), Black–brown (7), maroon (8), deep red (9), and red–brown (10). Because some of these colors, such as black–brown, maroon, deep red, and red–brown have a similar appearance, they are difficult to distinguish. False colors can enhance the color boundary between different pigments, and the UVRFC image shows obvious color differences between blue and bean-green areas. However, good color separation effects cannot be achieved for other color areas. The IRRFC images showed the boundaries of multiple color areas, and the UVL images illustrated the distribution of pigments with similar luminescent properties. The full-scene multi-band images depicting details of the mural are shown in Additional file 1. According to the results of our multi-band imaging surveys, the mural appears to have been painted using a mixing-and-layering process. Therefore, the instrumental analysis results of 10 representative color regions of the murals were extensively studied (Table 2). The multi-band images of 10 analysis points are shown in Figs. 3–6. Select instruments and methods were applied to examine these sampling points owing to the complementary analytical capabilities of the instruments and their different detection purposes. For example, non-destructive portable XRF analysis was performed on all 10 sampling points; samples were also collected for XRD and SEM–EDX analyses. Points (1), (5), (7), (8), (9) were sampled for SEM–EDS analysis. LC/M analysis was also performed on the sample at point (5), and m-RS analysis was performed on the sample at point

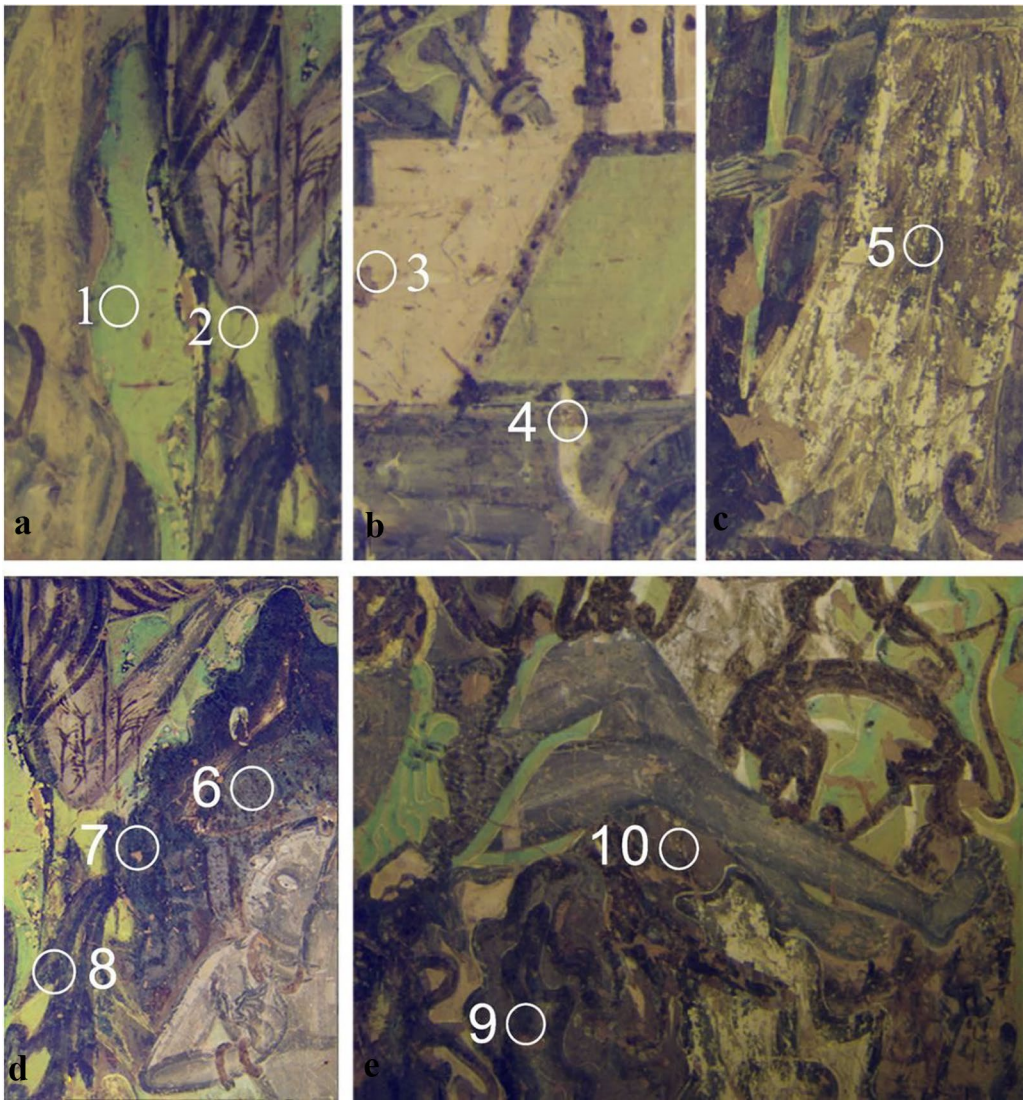

Fig. 5 Partial-view UVRFC imaging of the Prince Sattva mural and 10 analysis points

(8). A summary of the results of these analyses is shown in Table 3.

Blue and bean-green areas

The colors blue and bean-green cover wide parts of the mural, and their boundaries are difficult to distinguish in the VISR image (Fig. 3a [1, 2]). However, because the pigments used in these colors show different reflectances in the IR band, clearly delineating their boundaries in the IRRFC image is possible. The blue and bean-green pigments in the IRRFC image are violet and blue, respectively, (Fig. 4a [1, 2]). Although the delineation of pigment boundaries can be achieved, the direct identification of their origin using multi-band false-color images alone is not yet possible. The pDM observations indicate some layering and mixing between the blue and bean-green pigments (Figs. 7a [1] and 7a [2]). The pXRF results show that these two pigment areas contain high concentrations of Cu, followed by Fe and Ca (Fig. 7b [1, 2]). Microsamples of these pigments were used to prepare epoxy-embedded cross-sections. In the cross-sectional microscopic observations, mixing and layering could be observed between the blue and bean-green pigment particles, with the blue (layer 1) pigments lying on top of the bean-green (layer 2) pigments. The total thickness of these layers is 34.4 μm. A white 28.7 μm-thick layer (layer 3) is also present below the blue layer, the white pigment particles of which are sparsely mixed with the

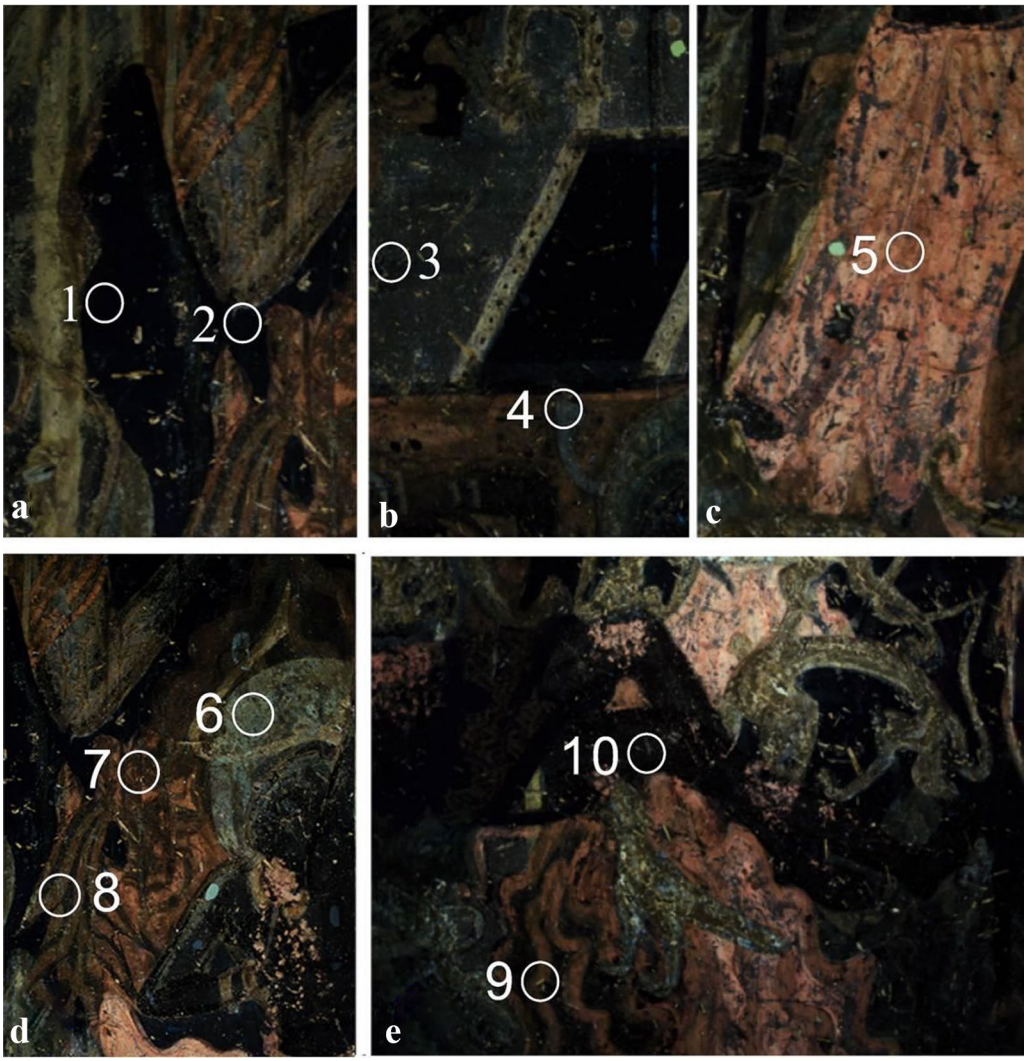

Fig. 6 Partial-view UVL imaging of the Prince Sattva mural and 10 analysis points

preparatory layer (Fig. 8a [1]). These three pigments make up a 34.0–55.0 μm-thick mixed-pigmented layer (Fig. 8b [2]). Based on the SEM–EDS analysis, the blue layer (layer 1) contains Cl, Cu, O, Si, Al, and K and the bean-green layer (layer 2) contains Cl, Ca, O, Cu, Si, Fe, Mg, Al, S, and K (Fig. 9-a). Based on the XRD analyses of micro-samples collected from the same locations, both sets of samples contain quartz [SiO_2], azurite [$Cu(CO_3)_2(OH)_2$], atacamite [$Cu_2Cl(OH)_3$], dioptase [$Cu_6Si_6O_{18}{\cdot}6H_2O$], and laumontite [$Ca(AlSi_2O_6)_2{\cdot}4H_2O$] phases. The bean-green samples also contain albite [$NaAlSi_3O_8$] and gypsum [$CaSO_4{\cdot}2H_2O$] phases (Figs. 10a, b).

By analyzing the aforementioned results, we can conclude that the blue and bean-green parts of the mural correspond to azurite and atacamite, respectively. The preparatory layer of these pigments is composed mainly of gypsum and clay.

White areas

The white pigment is mainly located in the pagoda in scene 5 and highlights, such as the clothes and skin of human characters (Fig. 3b [3, 4]). Because the reflectances of these white pigments are very similar, delineating their boundaries and determining their origin using multi-band images is quite difficult. In the IRRFC images, all of the white areas are milky white (Fig. 4b [3, 4]); in the UVRFC images, they are all cream colored (Fig. 5b [3, 4]). In the 365 nm-excited UVL images, the white areas show dim metallic-blue luminescence (Fig. 6b [3, 4]). Based on pDM observations, the white parts of the mural have

Table 2 Color description of mural pigments in the multi-band images

Test No	VISR < 400–700 nm <	H	S	B	IRRFC < 830 nm	H	S	B	UVRFC < 365–400 nm <	H	S	B	UVL Excitation: 365 Emission: 400–700 nm	H	S	B
1	Blue	218	23	43	Pink	346	17	48	Olive green	102	26	45	–	240	62	3
2	Bean green	185	16	60	Blue	213	26	53	Tea green	62	43	62	–	225	44	4
3	Ivory white	60	10	75	Milky white	51	7	77	Off white	42	35	74	Deep iron blue	192	29	14
4	White	41	10	72	Milky white	49	6	77	Off white	38	27	72	Deep iron blue	150	16	15
5	Light red	18	47	64	Pale lemon yellow	48	42	72	Dark brown	300	16	31	Salmon	16	48	66
6	Charcoal gray	36	6	35	Emerald black	168	54	36	Charcoal gray	266	13	43	Blue green	123	17	42
7	Black brown	11	33	26	Olive brown	47	40	42	Blue black	227	47	42	–	225	44	4
8	Maroon	16	46	44	Jade green	87	35	42	Charcoal gray	195	4	44	Salmon	23	58	57
9	Deep red	355	71	25	orange brown	38	63	36	Olive black	246	56	20	Salmon	20	55	42
10	Red brown	12	51	39	Black yellow green	59	52	50	Clay	16	24	31	–	0	14	3

This table denotes the false colors in the UVRFC and IRRFC images representing the current VISR colors of the mural. The HSB (H: hue, S: saturation B: brightness) values of each color are also indicated. The descriptions of the colors in the various images represent non-objective terms. The HSB color model can be used to describe and display the corresponding color objectively

Table 3 Summary of the main color-area findings

Analysis location	Current color	Global XRF	XRD analysis of the mixture	LC/MS	Pigment layer SEM–EDS	Pigment layer M-RS	Main pigment and stratigraphic sequence
NO. 1	Blue	Cu, Fe, As	Quartz, Azurite, Atacamite, Dioptase, Dickite, Laumontite	–	1: Cl, Cu, O, Si, Al, K 2: Cl, Ca, O, Cu, Si, Fe, Mg, Al, S, K	–	a. Azurite, b. Atacamite
NO. 2	Bean green	Cu, Fe, As	Quartz, Azurite, Atacamite, Dioptase, Dolomite, Laumontite, Albite, Gypsum	–	–	–	a. Atacamite, b.Azurite, c. Gypsum
NO. 3	Ivory white	Fe, Ca	Quartz, Gypsum, Talc, Lizardite, Hemihydrate, Gypsum, Clinochlore-1Mllb	–	–	–	a. Talc, Gypsum
NO. 4	Pure White	Pb, Fe	Quartz, Gypsum, Red lead, Clinochlore, PbO, Leucite, Felsobanyaite	–	–	–	a. Gypsum, b. Red lead, litharge
NO. 5	Light red	Fe, Pb, Ca, As	Quartz, PbO, Clinochlore, Gypsum, Felsobanyaite	Lac dye	1: Cl, Ca, Si, O, Fe, Na, Mg,Al K, C	–	a. Lac, b. Gypsum, c. Litharge
NO. 6	Charcoal grey	As, Hg, Fe, Ca	Quartz, Azurite, Gypsum, Dickite, Arsenolite	–	2: Cl, Ca, Si, Hg, As, Al, Mg,O, C, K, Fe 3: Cl, Ca, Si, Mg,As, Al, O, Fe, S, C	–	a. Realgar, Orpiment b. Gypsum
NO. 7	Black brown	Fe, As, Ca, Pb, Hg	Quartz, Carminite, Clinochlore, Illite, Cinnabar, Calcite	–	2: Ca, Fe, O, Si, Al, As, Mg, K, S	–	a. Cinnabar, b. Realgar, Orpiment, c. Calcite
NO. 8	Maroon	Fe, Pb, As, Ca	Quartz, Carminite, Clinochlore, Anorthoclase, Illite, Calcite	–	2: Cl, Ca, Si, Mg, O, Al, Fe, C 3: Cl, Ca, Si, As, Mg, O, Pb, Al 4: Cl, Ca, Si, Mg, O, Fe, Al, C, S	– 3.$PbCl_2$ 4.Pb_3O_4	a. Lac, b. Calcite, c. Realgar, Orpiment, d. Red lead
NO. 9	Deep red	Pb, Hg, As, Fe	Quartz, PbO, Calcite	–	2: Hg, Si, O, Al, As, C 3: Pb, O, C	–	a. Lac, b. Cinnabar, c. Litharge, d. Calcite
NO. 10	Red brown	Pb, Fe	Red lead, PbO	–	–	–	a. Red lead, b. Litharge

1,2,3, and 4 represent only the layers of the section, and the layers of the original paint pigment layers with a, b, c, and d

two different shades; the larger areas are painted in ivory-white (Fig. 7a [3]) while the local highlights are painted in pure-white (Fig. 7a [4]). The pDM observations also indicate that the ivory-white and pure-white parts have maroon and red-brown preparatory layers, respectively. Based on pXRF analysis, the ivory-white parts contain high concentrations of Fe, as well as Ca, while the pure-white parts contain high concentrations of Pb, as well as Fe (Figs. 7b [3] 4). As the stratigraphy of the ivory-white pigments is relatively simple, we only prepared an epoxy-embedded cross section of the pure-white pigment. This cross section showed a pure-white pigment layer measuring approximately 25.0 μm in thickness lying on top of a red–brown preparatory layer (Fig. 8c [4]). Based on XRD analysis, the ivory-white areas are painted with a clay-mineral pigment predominantly consisting of talcum [$Mg_3Si_4O_{10}(OH)_2$] and containing quartz [SiO_2], gypsum [$CaSO_4{\cdot}2H_2O$], lizardite [$(Mg_3Si_2O_5(OH)_4$], hemihydrate gypsum [$CaSO_40.5H_2O$], and clinochlore [$Mg_5Al(AlSi_3O_{10}(OH)_8$] (Fig. 10c). The pure-white areas are painted with a clay-mineral pigment that mainly consists of gypsum [$CaSO_4{\cdot}2H_2O$], albite [$NaAlSi_3O_8$], leucite [$KAlSi_2O_6$], and felsobanyaite [$Al_4(SO_4)(OH)_{10}{\cdot}4H_2O$] (Fig. 10d). The pure white sample also shows intense red lead [Pb_3O_4], litharge [PbO], and arsenolite [As_4O_6] phases [40]. These components most likely originated from the red-brown pigment and preparatory layer, which serve as the mural's background and preparatory layer. Therefore, a pigment layer consisting of a mixture of red lead and litharge should be found below the pure-white pigment. This layer is actually the background color of the mural, and the pure-white pigment is painted directly over it. The red-brown background will be further described in detail in a later section.

Light-red areas

The light-red pigment appears in scenes 1–3 on the clothes of human characters and some mountains (Fig. 3c

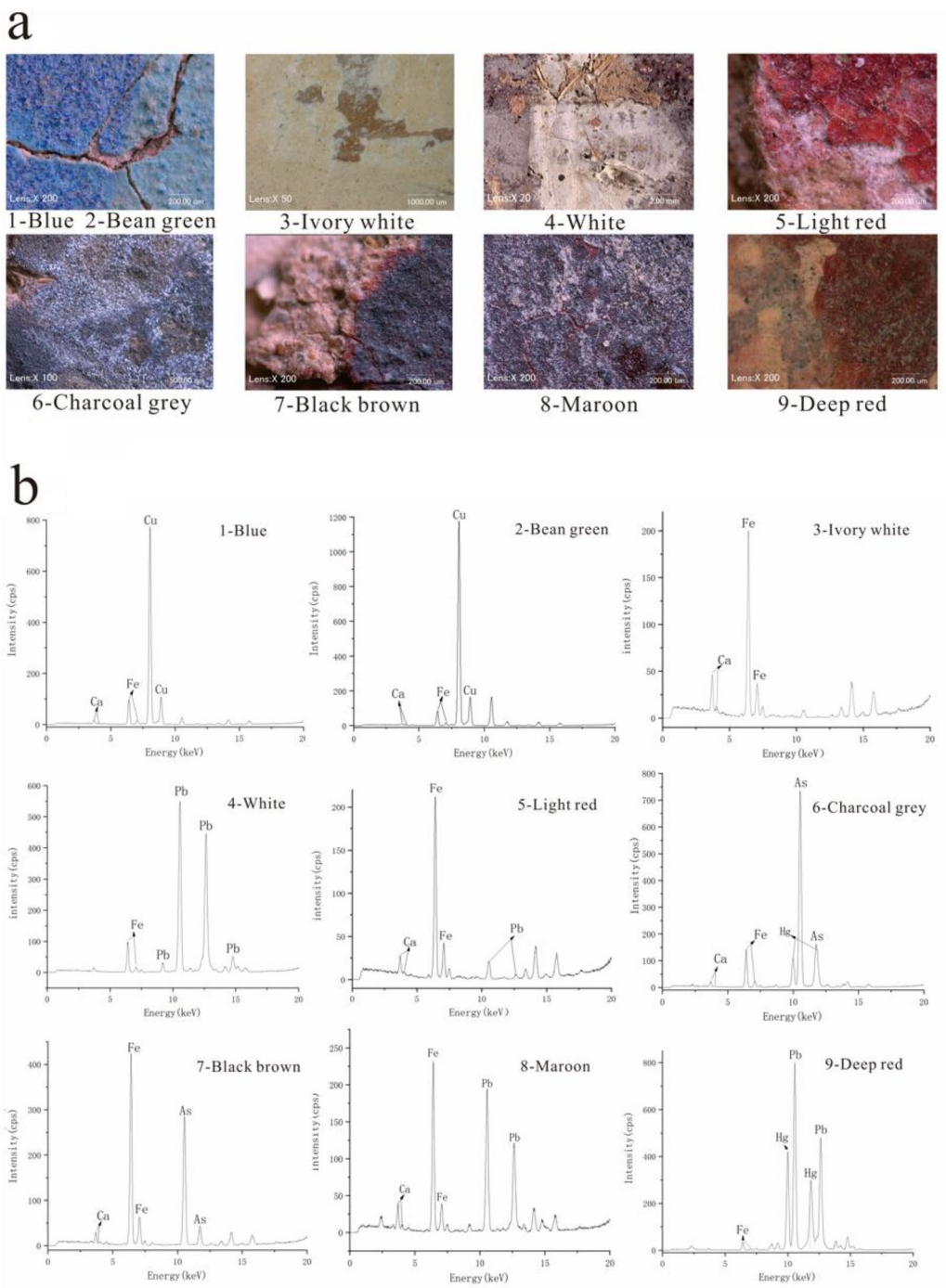

Fig. 7 Noninvasive XRF analysis of nine color-areas: **a** microscopic images of the nine XRF-analyzed areas and **b** the corresponding XRF spectra

(See figure on next page.)

Fig. 8 Cross-sectional microscopy images of microsamples from nine color-areas. Note: 1, 2, 3 and 4 represent the layers of the section

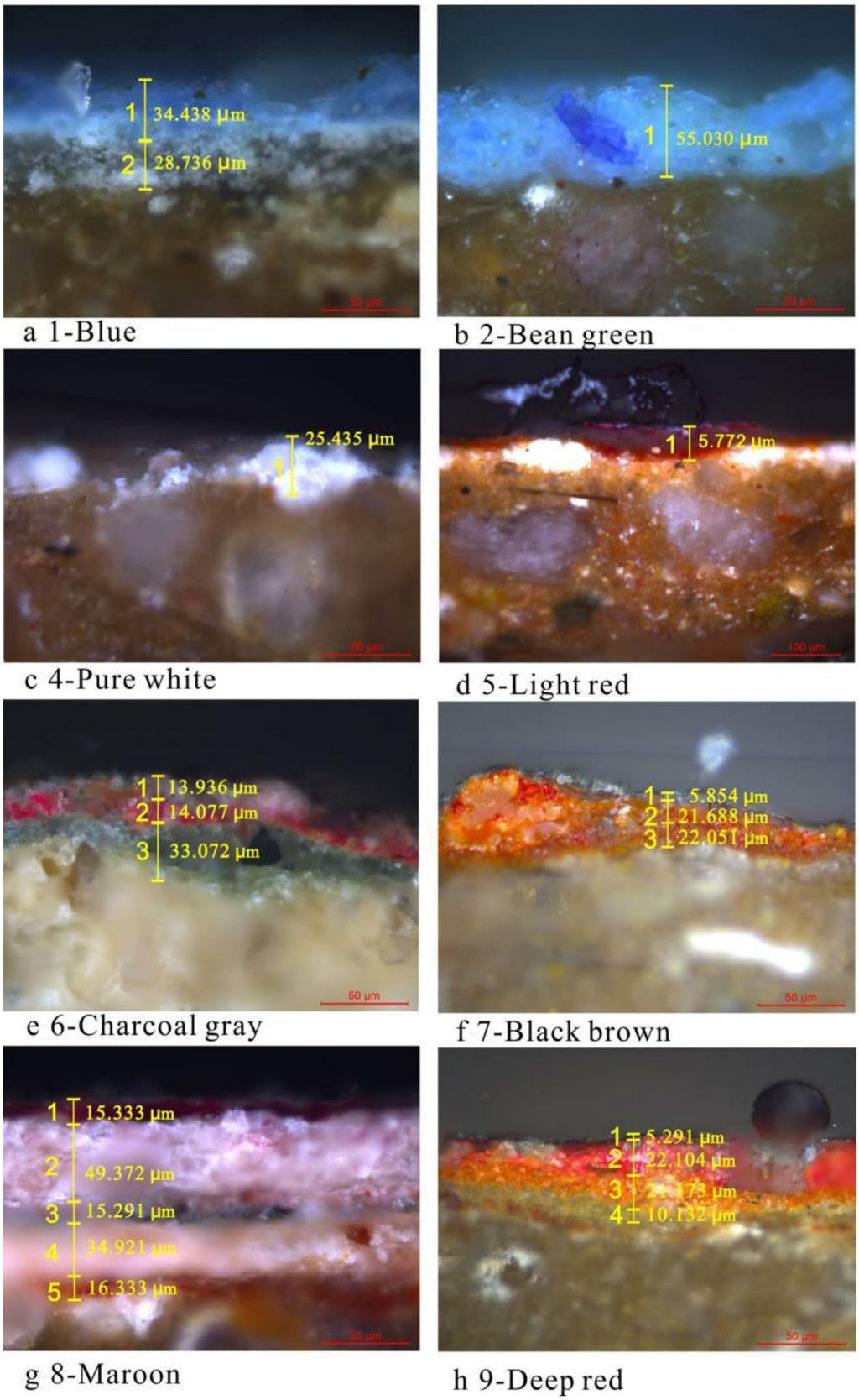

Fig. 8 (See legend on previous page.)

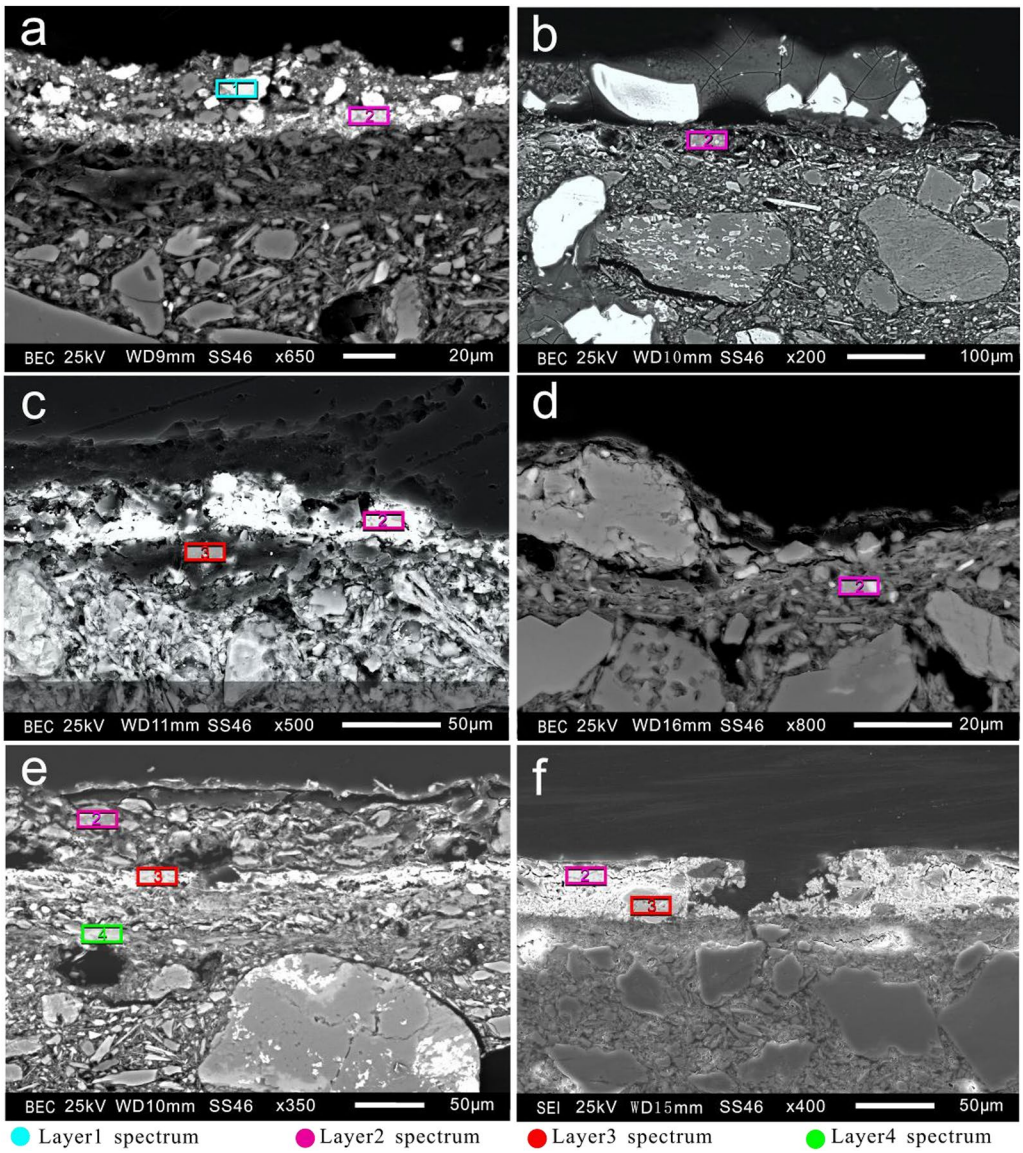

Fig. 9 SEM–EDS analysis of cross-sectional samples taken from nine overlapping color-areas: **a** Blue + bean green, **b** light red, **c** charcoal gray, **d** black–brown, **e** maroon, **f** deep red. Note: The SEM–EDS spectrum corresponding to the analyzed points of a specific layer are marked in violet, red, or green. 1, 2, 3 and 4 represent the layer sequence and the analysis points of the layers of these sections. The SEM images are correlated in sections a, d, e, f, and g in Fig. 8. See Supplementary Materials 3 for the EDS spectra

[5]). The light-red pigment is light lemon yellow in the IRRFC image (Fig. 4c [5]) and emits an intense salmon luminescence in the 365 nm-excited UVL image (Fig. 6c [5]). This finding indicates that organic paint may be present in the light-red parts of the mural. The deep-red pigments and some maroon pigments (which will be discussed in later sections) also exhibit this type of luminescence. pDM observations of a damaged part of the mural show bright-red, white, light-red, and yellow pigments, as well as an earthen ground layer (Fig. 7a [5]). The pXRF analysis shows that this region has high concentrations of Fe, Pb, and Ca (Fig. 7b [5]). In the cross-sectional pigment sample, the light-red area consists of a 5.7 μm-thick red pigment layer that covers the white and yellow pigment layers(Fig. 8d [5]). The SEM–EDS analysis indicates that the bright-red layer contains Cl, Ca, Si, O, Fe, Na, Mg, Al, K, and C (Fig. 9b). The XRD analysis shows that the light-red parts of the mural contain quartz [SiO_2], litharge[PbO], clinochlore [$Mg_5Al(AlSi_3)O_{10}(OH)_8$], gypsum [$CaSO_4{\cdot}2H_2O$], and felsobanyaite [$Al_4(SO_4)$

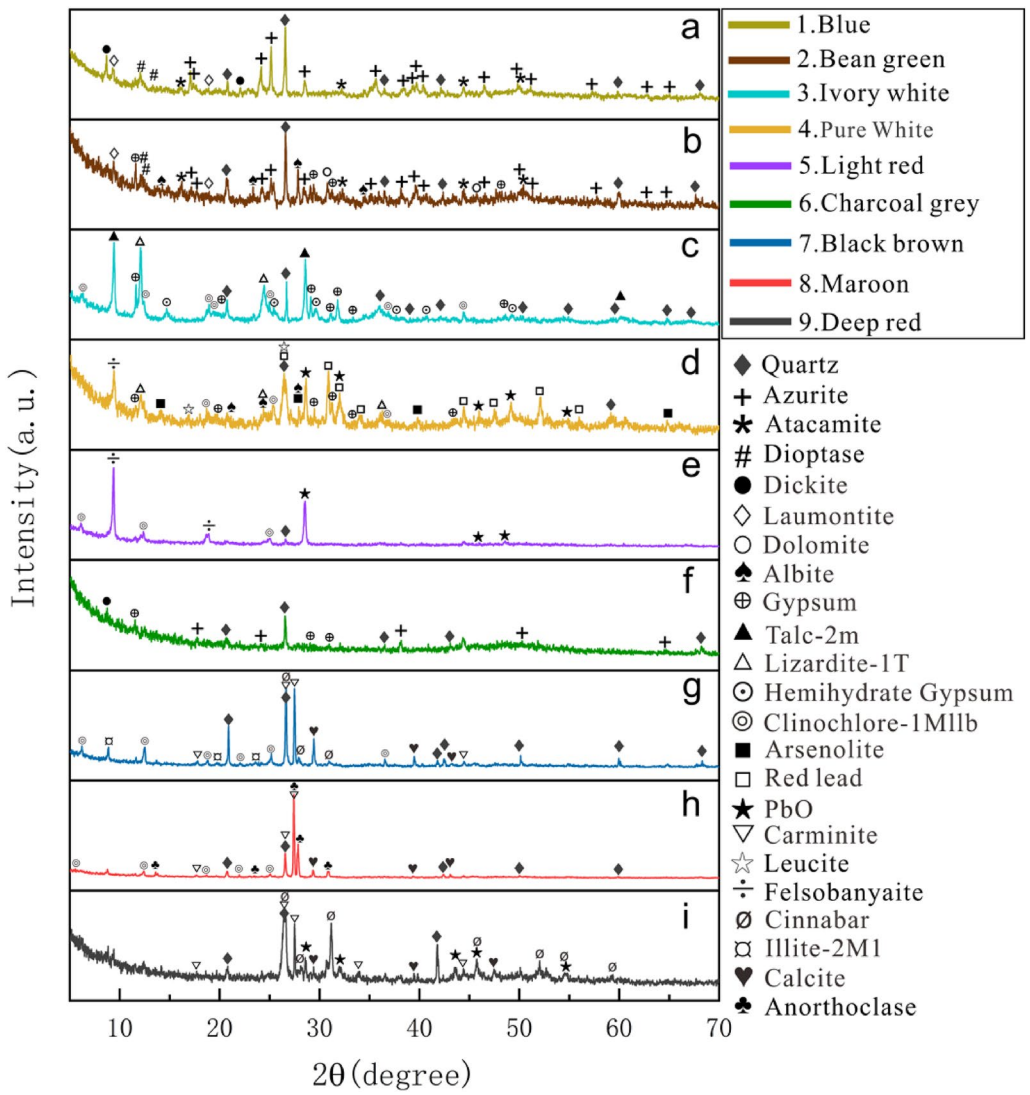

Fig. 10 XRD analysis of pigment samples from nine color-areas

$(OH)_{10}{\cdot}4H_2O$] phases (Fig. 10e), with litharge and felsobanyaite possessing the most intense diffraction peaks. Therefore, the yellow pigment in the pigment mixture is mainly litharge, and the white pigment is white gypsum-dominated clay-mineral mixture.

LC–MS analysis was performed on the light- and deep-red pigments producing salmon luminescence. The shellac-related compounds detected in the pigment samples included shellolic acid, oxidized shellolic acid, jalaric acid, aleuritic acid, jalaric acid ester and 16-hydroxyhexadecanoic acid [41]. The retention time of laccaic acid A was observed to be 5.72 min from the EIC of the $[M-H]^-$ ion at m/z 536.0840 ($C_{26}H_{19}NO_{12}$). In the MS2 spectrum, the precursor ion was further fragmented to $[M-H-CO_2]^-$ at m/z 492.0943, $[M-H-2CO_2]^-$ at m/z 448.1038, and $[M-H-2CO_2\text{-}H_2O]^-$ at m/z 430.0930. Therefore, we can infer that the compound also contains laccaic acid A [42, 43]. The above results suggest that the pigment samples in the light-red areas contain shellac. Our discovery of laccaic acid A can serve as an important reference that the light-red in the murals is derived from lac pigments prepared from shellac. Salmon-colored luminescent mural samples from other regions were analyzed by LC–MS with similar results (Fig. 11[a–b] and Additional file 1). The main components of these pigment samples and their retention times, molecular ion peaks and high-energy collision fragments are given in Table 4.

The XRD analysis showed that the felsobanyaite was composed of potassium aluminum sulfate dodecahydrate [$KAlSO_4{\cdot}12H_2O$], which is a crystal formed via

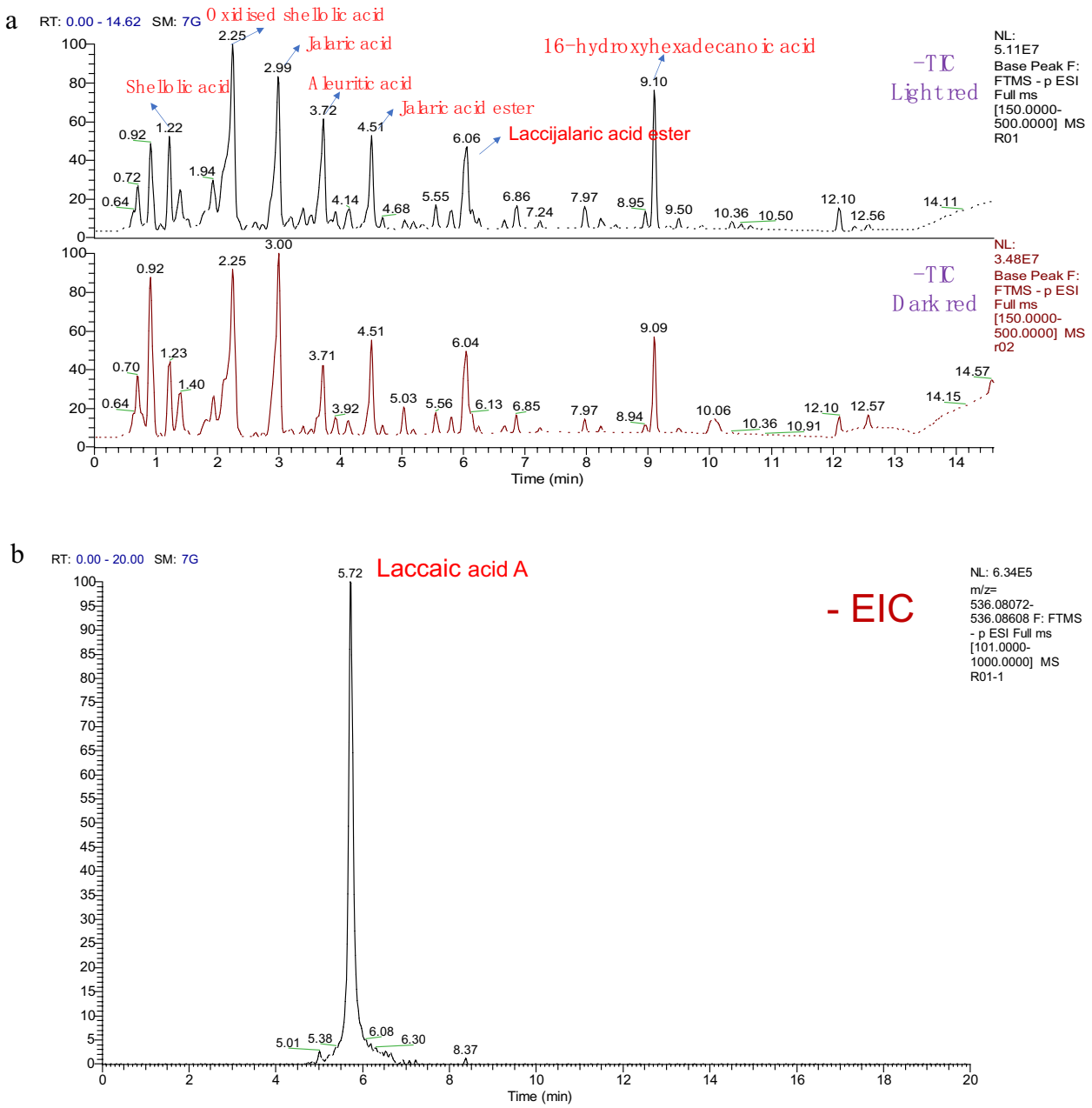

Fig. 11 LC–MS analysis of pigment samples from sampling point 5 and point 9 with salmon luminescence. **a** Total ion chromatograms. **b** Extracted ion chromatograms of m/z = 536laccaic acid A

the processing and refinement of alunite. The presence of K, Al, Na, S, O, and C indicated that the lac pigments in the mural surface was prepared as a lac by combining water-soluble shellac with alkaline potassium alum [$KAlSO_4{\cdot}12H_2O$] [44, 45]. The colors pink, red, and purple can be formed by the addition of different metal salts to the lac pigments. The intense light-red hue of the mural may be produced by a lac lake compound. However, lac lake only produces very weak luminescence when irradiated with 365 nm light in the laboratory setting. The intense salmon-colored luminescence in the murals may be due to lac residue from the shellac preparation process [46].

The comprehensive results show that the light-red areas are composed of a top layer consisting of lac pigments, a second layer consisting of gypsum, clinochlore,

Table 4 LC/MS detection of pigment samples in the salmon luminescent region

Compound	Molecular formula	Rt/min	Molecular ion peak [M-H]- m/z	Fragment ions (m/z)
Shellolic acid	$C_{15}H_{20}O_6$	1.22	295.1185	251.1286/249.1133/177.1284/121.0650
Oxidized shellolic acid	$C_{15}H_{18}O_6$	2.25	293.1027	249.1129/205.1234/109.0659/83.0503
Jalaric acid	$C_{15}H_{20}O_5$	2.99	279.1235	261.1129/235.1335/217.1230/147.0449/119.0503
Aleuritic acid	$C_{16}H_{32}O_5$	3.72	303.2176	285.2070/267.1967/201.1138/171.1024/127.1125
Laccaic acid A	$C_{26}H_{18}O_{12}N$	5.72	536.0840	492.0943/448.1038/430.0930
Jalaric acid ester	$C_{24}H_{33}O_9$	4.51	465.2125	277.1078/187.0973/233.1180/147.0450/465.2130
16-hydroxyhexadecanoic acid	$C_{16}H_{31}O_3$	9.10	271.2276	271.2274/225.2220/253.2168/141.1281/113.0972

The figures in the table are all experimental values

and quartz (a white clay-mineral mixture), and a third layer consisting of litharge.

Charcoal-gray areas

Many parts of the mural show charcoal-graying. A representative example of this feature is the oval halo behind the prince's head in Scene 2 (Fig. 3d [6]). The IRRFC image displays in black–jade green (Fig. 4d [6]) and emits green luminescence in the 365 nm-excited UVL images (Fig. 6d [6]). The pDM image shows a grayish-white layer over the pigment, the superposition of which results in a charcoal grey visual effect (Fig. 7a [6]). The pXRF analysis indicates that this area has a high As content, as well as small amounts of Hg, Fe, and Ca (Fig. 7b [6]). A cross-sectional sample indicated the presence of a 13.9 μm-thick grayish-white surface cover (layer 1), a 14.0 μm-thick deep-red pigment layer (layer 2) that also contains a small number of orange particles, and a 33.0 μm-thick olive-green pigment layer (layer 3) that also contains a small number of white particles (Fig. 8e [6]). The EDS analysis of layer 2 with obvious pigments revealed that this layer contains Ca, Hg, Si, O, K, Fe, C, Al, Mg, and As. Layer 3 contains Cl, Ca, Si, Mg, As, Al, O, Fe, C, and S (Fig. 9c). The XRD analysis of the pigment samples showed quartz [SiO_2], azurite [$(Cu_3CO_3)_2(OH)_2$], gypsum [$CaSO_4{\cdot}2H_2O$], dickite [$Al_2Si_2O_5(OH)_4$], and arsenolite [As_4O_6] phases (Fig. 10f). The presence of azurite in the charcoal-gray samples is due to contamination by the surrounding blue pigments; the charcoal-gray areas themselves are not actually painted with blue pigments.

In summary, Layer 1 is composed of arsenolite, which could be attributed to the oxidation of arsenic sulfide or hydrolysis of arsenic chloride. High concentrations of Cl, As, and S in the pigment layer promote the oxidation reaction. In addition, Cave 254 was open for a long time in history, resulting in its extensive exposure to sunlight. It also suffered severe fire damage. Extended periods of exposure to sunlight and high temperatures may have sped up the oxidative degradation and color changes of sulfide pigments in the mural [47]. This phenomenon has been reported in the literature. For example, the oxidation of orpiment (As_2S_3, golden yellow) converts it to arsenic oxide (As_2O_3, gray or white) and the oxidation of realgar (a-As_4S_4, orange-red) converts it to pararealgar (b-As_4S_4, yellow) and then to arsenic oxide [20]. Arsenolite is a dimorph of As_2O_3. Therefore, it can result from the oxidation of a mixture of realgar [a-As_4S_4] and orpiment [As_2S_3] and cause the discoloration of the pigment; arsenite is an intermediate product of this oxidation process. All areas in which arsenite appears emit varying degrees of green luminescence; while the exact source of this luminescence is unknown, it helps identify the locations of arsenic pigments in the mural.

Layer 2 represents the topmost pigment of the original painting and is originally composed of realgar and orpiment compounds, with orange particles still visible in the cross-sectional sample. The deep-red pigment shown in the profile is not a ubiquitous pigment in the charcoal-gray areas, but comes from the superimposition of cinnabar and realgar at the sampling location.

Layer 3 seems to be composed of clinochlore. The compound is iron-rich chlorite and may be related to ferroan clinochlore. The crystals range from transparent to translucent, and olive green is part of the colors. This compound was reported to be formed by the alteration of arsenate and ferromanganese minerals mixed with quartz and dickite; it is often combined with other materials as a painting preparatory layer [48–50]. Unfortunately, XRD analysis failed to detect significant clinochlore phases in the trace samples, possibly because the low concentration of these phases or pigment mixtures leads to signals blocked by the background noise or strong reflections from other substrates. The high content of Ca and some white particulate matter in this layer indicates that gypsum was mixed with it.

According to the above analysis, the original coating of the charcoal-gray area is composed of a compound

pigment (realgar and orpiment-related compounds) and a preparatory layer of gypsum mixed with plagioclase and dickite.

Brown areas

Inspection of the brown parts of the mural indicated that they consisted of three hues: black–brown, maroon, and red–brown. The black–brown parts are located on human clothes and mountains. Many parts of the mural are colored maroon, including the mountains, skin and clothes of the human characters, and the area with holy lights behind the human characters' heads. The red–brown parts are located in the background. As the color and appearance of the black–brown and maroon parts are very similar, delineating their color boundaries in the VISR image (Fig. 3d [7, 8]) is difficult. However, the IRRFC image shows a small difference in the IR reflectance of these color areas. In the IRRFC image, the black–brown parts are shown in olive–ochre (Fig. 4d [7]), while the maroon parts are shown in jade green (Fig. 4d [8]). In the 365 nm-excited UVL image, the dark-brown area has a weak salmon luminescence similar to that of the light-red area (Fig. 6d [7, 8]) (full-scene multiband image A1 in Additional file 1). Microsamples were obtained from damaged parts of the mural in Scene 2 (i.e., the black edges of the mountain range and the dark-brown pigment layer on the edges of the human characters' clothes). Extensive pXRF investigations were also performed on the red–brown area.

Black–brown area

Based on the pDM observations, the black–brown area has a dark-brown pigment layer covered by a layer of black–gray matter (Fig. 7a [7]). The pXRF analysis shows that the black–brown area contains high concentrations of Fe and As, as well as Ca (Fig. 7b [7]). Based on microscopic observations of the cross-sectional samples, a 5.8 μm-thick black–gray layer covers 21.6 and 22.0 μm-thick layers of pigment mixtures consisting of yellow and red particles (Fig. 8f [7]). According to the SEM–EDS analysis, the red–yellow pigment mixture (layer 2) contains Si, Ca, Fe, Mn, O, Al, As, Mg, Ca, and K (Fig. 9d). The XRD analysis of the microsample revealed the presence of quartz [SiO_2], carminite [$PbFe_2(AsO_4)_2(OH)_2$] [51], clinochlore [$Mg_5Al(AlSi_3)O_{10}(OH)_8$], cinnabar [HgS], illite [$(K,H_3O)(Al,Mg,Fe)_2(Si,Al)_4O_{10}(OH)_2{\cdot}(H_2O)$], and calcite [$CaCO_3$] phases (Fig. 10g).

The discovery of carminite (a Pb–Fe hydroxyarsenate belonging to the orthorhombic crystal class) in the black–brown area was somewhat unexpected, as it is a rare secondary mineral. The optical appearance of carminite is generally described as carmine or reddish yellow [52, 53]. Indeed, the use of carminite as a pigment would be a very interesting discovery for the technological history of China. Although mimetite, an arsenite, is well known to be used as a paint in the Dazu Rock Carvings in China [54], reports on the direct use of carminite as a mural paint are rare. Carminite is most likely a product of sulfide and arsenide oxidation [55]. Based on tests conducted by the National Museum of American History on pure carminite samples from Mapimi (Mexico), the theoretical composition of the accepted formula of carminite includes PbO, CaO, MgO, FeO, Fe_2O_3, Al_2O_3, As_2O_5, P_2O_5, and water [56]. The elemental composition of As, Fe, O, Al, Mg, and Ca in the mixed red–yellow pigment layer is consistent with the elemental composition of carminite. Changes in temperature and humidity could reduce sulfur-containing compounds, increasing their susceptibility to oxidation. This state leads to the formation of Hg-As oxides or hydroxide and sulfate minerals [57]. Because carminite is an O-containing salt, it is likely to be an intermediate product of cinnabar and realgar oxidation. If this hypothesis is correct, the red–yellow mixture should consist of cinnabar (red), carminite (red), realgar (As_4S_4), and pararealgar (b-As_4S_4) (yellow), of course, it cannot be ruled out that there is a concomitant state of Orpiment [58]. The red and yellow colorations most likely originated from cinnabar and a mixture of realgar with orpiment (which was originally orange), respectively. Owing to their crystalline properties, these pigments are incompatible with each other in a painting. Cinnabar was painted on top of a layer of mixture of realgar with orpiment; however, as the crystal grains of these pigments have different specific gravities, the pigments eventually mixed with each other. The black–gray matter on the surface could be the final product of arsenic sulfide oxidation, which indicates that As ions migrated through the pigment layers during mural degradation. These findings also imply that this process began from the pigment surface. The preparatory layer is a white clay-mineral pigment mainly consisting of quartz and calcite, which also contains clinochlore and illite.

Maroon and red–brown areas

Based on our extensive pXRF investigations, we discovered that the red–brown area contains high concentrations of Pb and Fe. In the IRRFC images, the red–brown area appears dark yellow–green. As mentioned earlier, the red–brown background consists mainly of red lead and litharge.

A detailed investigation was conducted on the maroon areas. The pDM observations show that a layer of pink matter covers another layer of maroon pigment (Fig. 7a [8]). The pXRF analysis shows that the maroon areas contain high concentrations of Fe,

Pb, and Ca (Fig. 7b [8]). Cross-sectional microscopy indicated that the maroon areas are composed of a total of five pigment layers: a 15.3 μm-thick maroon layer (layer 1), a 49.3 μm-thick white–maroon mixture (layer 2), a 15.2 μm-thick dark-gray layer (layer 3), a 34.9 μm-thick white–orange mixture (layer 4), and a 16.3 μm-thick orange-red mixture (layer 5) (Fig. 8g [8]). The SEM–EDS analysis showed that the second layer contains Cl, Ca, Si, Mg, O, Al, Fe, and C; the third layer contains Cl, Ca, Si, As, Mg, O, Pb, and Al; and the fourth layer contains Cl, Ca, Si, Mg, O, Fe, Al, C, and S (Fig. 9e). According to the XRD analysis of microsamples taken from the same positions, the maroon areas contain quartz [SiO_2], carminite [$PbFe_2(AsO_4)_2(OH)_2$], microcline [$(Na,K)AlSi_3O_8$], illite [$(K,H_3O)(Al,Mg,Fe)_2(Si,Al)_4O_{10}(OH)_2\cdot(H_2O)$], and calcite [$CaCO_3$] phases. The signals of the carminite, microcline, and quartz peaks are especially strong (Fig. 10h). Because of the complexity of the formation, the high-resolution spectral information of the pigment layers at different depths of the finite samples was obtained by using m-RS. Based on Raman fingerprinting, the white particles contain lead chloride ($PbCl_2$), while the orange–red particles contain red lead (Pb_3O_4) (Additional file 1). Combining these results with those of the EDS analysis revealed that these components came from the third and fourth layers.

The pigments in the inspected maroon-colored points show a weak luminescence that is identical to that of the light-red and deep-red areas. As mentioned in the previous shellac analysis, lac components were also found in these points. This layer is partially mixed with the second layer, which is a calcite-dominated clay-mineral preparatory layer, the purpose of which is to enhance the hue of the lac pigments and prevent mixing with the underlying pigment layers. Layer 3 may have been formed by the oxidation of S, As, and Pb due to their contact with the aforementioned mixture. The results of the elemental analysis indicate that the elements and colors of the mixing layer between the fourth (white) and fifth (orange–red) layers are similar to those of carminite. Therefore, the products of sulfide and arsenide oxidation could be present in these layers, i.e., the oxidation products of realgar [As_4S_4] and orpiment [As_2S_3]. Owing to the migration of As ions between the third, fourth, and fifth layers, these ions form an oxide with Pb ions from the third layer, resulting in the formation of a dark-gray layer. Thus, the initial pigment layer in the maroon areas, from top to bottom, may consist of only four pigments, namely lac pigments, calcite, a mixture of realgar and orpiment, and red lead. Lead chloride may be used as an extender for As-based pigments.

Deep-red areas

The deep-red and brown areas have a similar color and appearance, and the former is mainly located at the edges of the mountains in the mural (Fig. 3e [9]). In the IRRFC image, the deep-red areas are orange–brown in color (Fig. 4e [9]). In the 365 nm-excited UVL image, the deep-red areas have salmon luminescence that is identical to that of the light-red areas (Fig. 6e [9]). The pDM observations of a damaged part of the mural reveal a layer of orange–red pigment covering a soil base, as well as a layer of deep-red pigments (Fig. 7a [9]). The pXRF analysis shows that this region contains high concentrations of Pb and Hg, as well as some Fe (Fig. 7b [9]). The cross-sectional microscopic images show that the deep-red areas consist of four stacked pigment layers: a 5.2 μm-thick deep-red layer (layer 1), 22.1 μm-thick red layer (layer 2), 21.2 μm-thick orange–yellow layer (layer 3), and 10.1 μm-thick soil-yellow layer (layer 4) (Fig. 8-h). The SEM–EDS analysis shows that the second layer contains a high concentration of Hg, as well as Si, O, Al, As, and C. The third layer has a high Pb content, as well as some O and C (Fig. 9f). In the XRD analysis of microsamples from the deep-red area, quartz [SiO_2], carminite [$PbFe_2(AsO_4)_2(OH)_2$], litharge [PbO], cinnabar [HgS], and calcite [$CaCO_3$] phases were detected (Fig. 10i).

Based on the results above, we can deduce that the pigment layers of the deep-red area contain lac (layer 1), cinnabar (layer 2), and litharge (layer 3). The preparatory layer was made of calcite.

Stratigraphy of the pigment layers

When painting a mural, the layering or mixing of pigments is often necessary to create a desired color or effect. Although the concept of "chemistry" had not been formalized in ancient China, the stratigraphy of the pigment layers revealed that the ancient artists of China understood the concept of chemical compatibility, specifically that some pigments can be chemically compatible or incompatible with each other. In our analyses, we found that the mineral pigments in the mural include azurite, atacamite, red lead, realgar, and orpiment-related compounds, cinnabar, gypsum, talc, calcite, and organic dyes, such as lac (Fig. 12).

First, gypsum and calcite were used to create the preparatory layer. However, these white pigments are not used in all areas where the color-pigment layer is in contact with the preparatory layer. Instead, their usage depends on the refractive characteristics of the crystal grains of the color-pigment. They are also used to separate pigment layers that are chemically incompatible with each other. This approach allows the artist to enhance the pigment color while keeping incompatible pigments isolated from each other. For example, gypsum was used

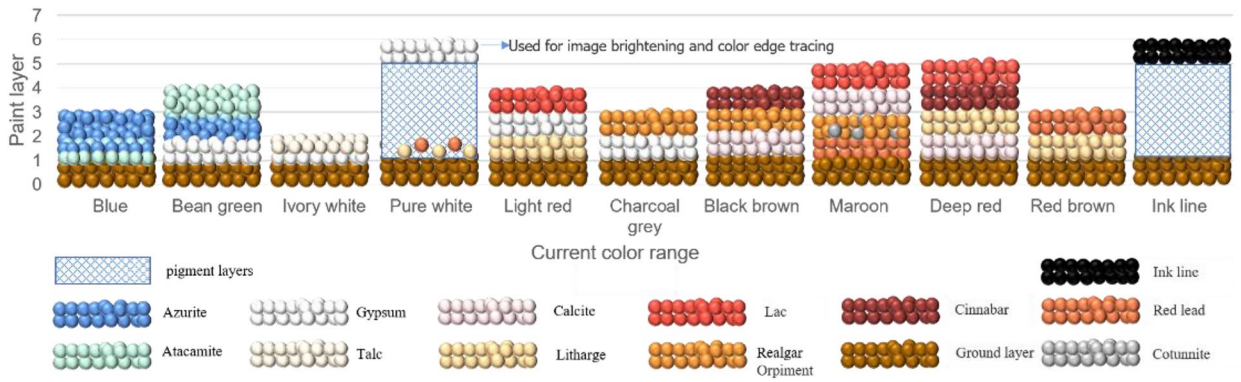

Fig. 12 Model of pigment stratigraphy. Horizontal axis: current colors of the mural's pigments; vertical axis: pigment layers

below azurite (a Cu-based pigment) to separate it from the alkaline soil in the ground layer [59], thus preventing the pigment color from changing owing to reactions with the alkaline soil. Using gypsum as a preparatory layer could also flatten the preparatory layer and enhance the color of the azurite pigment. Gypsum was further used as a preparatory layer when As-based pigment was in contact with the base. In areas where the lac dye comes into contact with the litharge, gypsum was used to separate the pigment layers, lighten the redness of the lac dye, and prevent the Pd-based pigment from darkening due to moisture.

Calcite is even more chemically stable and, thus, has better refractive properties than gypsum owing to its crystalline nature. When used as a barrier layer, calcite prevents chemical reactions between chemically incompatible pigments while allowing their colors to mix. In the mural, calcite was used as a barrier layer between the preparatory layer and As-based pigment, between lac and As-based pigment, and between litharge and the ground layer. Talc, which has a smooth texture, can be applied with gypsum to enhance the adhesion of the preparatory layer to the soil base. Talc was used to create the surface of the pagoda in Scene 5, giving the pagoda a luster that resembles white jade.

Second, pigment incompatibilities will accelerate their oxidation and color change. Cu-based pigments, such as azurite and atacamite, were never layered with Pb-based pigments, such as red lead and litharge, or As-based pigments, such as realgar or orpiment, to avoid this issue. Moreover, no contact between As-based pigment and red lead or between cinnabar and red lead was observed. Despite these precautions, however, the pigments in the mural still showed varying degrees of color change and fading. These changes are known to be very complex, as they are driven by a multitude of intrinsic (pigment properties) and extrinsic (the surrounding environment and microbes) factors. The international literature includes a large body of research on pigment compatibility [60], which has proven to be invaluable for determining pigment compatibilities.

Pigment-painted areas and digital reconstruction

By projecting the pigment analysis results to pigment features in the multi-band images, we can determine the distribution of each pigment in the mural (Fig. 13[a–j]). The HSB values of each pigment were determined using the VISR images of newly purchased pigment samples (Fig. 13k). These values were subsequently used to digitally reconstruct the original colors of the mural. In the digital reconstruction, the ideal colors of the pigments were simulated under normal conditions (Fig. 14). Based on the stratigraphy of the painted layers, the painting process was likely to involve 12 steps: (1) drawing of structural lines, (2) coloring with litharge, (3) coloring with red lead, (4) laying of the gypsum base, (5) coloring with azurite (6) coloring with atacamite, (7) laying of the calcite barrier, (8) coloring with realgar and orpiment- related compounds, (9) coloring with cinnabar, (10) coloring with lac dye, (11) inking of lines, and (12) brightening of highlights (such as white areas on human bodies, organs, clothes, and decorations).

The coloring of human bodies in the mural was performed using a technique called the "convex-and-concave method" (*aotufa*), where gradual changes in color are used to create a sense of three dimensionality. This technique was especially popular during the Northern Wei Dynasty, and can be observed in, for example, part of the mural in the south wall of the cave 260 (386–534) of the Mogao Grottoes, where a less-damaged mural that was once covered with mud was found (Additional file 1). It is performed by using a deeper color on the inner edge of a contour and then gradually transitioning to a lighter color toward the outer edge, causing limbs to appear

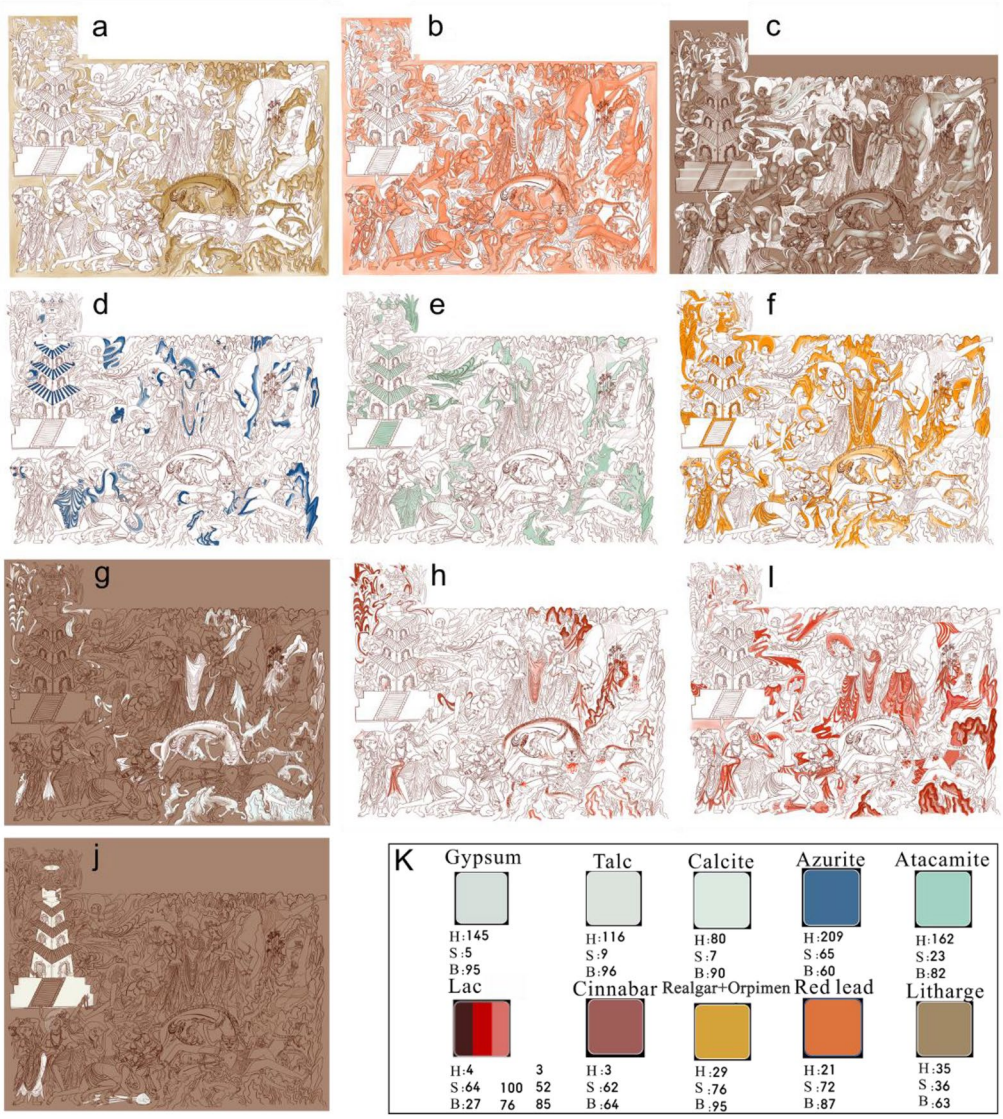

Fig. 13 Areas in which each pigment was used and their hue. **a** Litharge, **b** red lead, **c** gypsum, **d** azurite, **e** atacamite, **f** realgar, **g** calcite, **h** cinnabar, **l** lac, and **j** talc. **k** VISR palette and HSB values of the pigments used in the mural

more 3D-like. Prominent parts of the human characters' face, such as the forehead, eyebrows, eyes, bridge of the nose, chin, and middle of the face, are highlighted using white paint. This style of painting proves that the introduction of Indian Buddhist art to China around the fourth century CE had a significant influence on early murals in the Mogao Grottoes. This technique continued to be used in the murals of the Mogao Grottoes until the end of the Tang Dynasty (618–907 CE), at which point a decorative style came to prominence.

Conclusion

In this study, a Northern Wei Dynasty mural in the Mogao Caves was extensively and in-depth analyzed to create a digital reconstruction that provides related information on its pigment types, painting patterns, and

(See figure on next page.)

Fig. 14 Digital reconstruction of the Prince Sattva mural. **a** Reconstruction of the line drawing, **b** color reconstruction, and **c** partial features of the mural without discoloration in Cave 260 of the Northern Wei Dynasty in the Mogao Grottoes

Fig. 14 (See legend on previous page.)

original colors. The relationship between painting processes and pigment degradation (color change and fading) was also described. Technical photography helped restore the details of the faded image and enriched the cognitive value of mural art.

The pigment analysis mainly confirmed the application of lac pigments in the murals. The salmon luminescence in the UVL images originated from shellac residue added during the preparation of lac pigments. The oxidation of pigments containing As, Pb, and Hg led to the production of new compounds, such as arsenolite and Pb–Fe hydroxyarsenate. Ultimately, these findings improve the relative objectivity of virtual reconstruction. The final virtual reconstruction demonstrates that our methods represent a promising approach for art conservation and studies. However, differences in pigment origin and the size or selection of binders and the level of imitation of the artist's personal style may affect the final virtual reconstruction of the mural. The exact identity of some color-changing pigments and the reasons behind their change must also be determined to enhance the objectivity of restoration. Despite these limitations, these are valuable to understand the painting process of murals in Northern Wei Dynasty light for further study.

In future work, we aim to improve the analytical methods and approaches used for our virtual reconstruction. We will also employ advanced technologies, such as neural network and machine learning, to recreate the process by which the mural degraded from its original appearance to its current state.

Abbreviations

MSI: Multi-band imaging; VISR: Visible-reflected; IRR: Infrared-reflected; IRRFC: Infrared-reflected false color; UVL: Ultraviolet luminescence; UVR: Ultraviolet-reflected; UVRFC: Ultraviolet-reflected false color; VIL: Visible light-induced infrared luminescence; VIVL: Visible light-induced visible luminescence; pXRF: Portable X-ray fluorescence analyzer; SEM/EDX: Scanning electron microscopy/energy dispersive X-ray spectroscopy; LC/MS: Liquid chromatography/mass spectrometry; pDM: Portable digital microscope; m-RS: Confocal Raman microspectroscopy; UNESCO: United Nations Educational, Scientific and Cultural Organization.

Supplementary Information

The online version contains supplementary material available at https://doi.org/10.1186/s40494-022-00785-4.

Additional file 1. Multi-band image reference files for pigment samples. The table1.1 is the multi-band images of the pigment samples, and Table 1.2 is the pigment samples source of the multi-band image reference files.

Acknowledgements

This research received strong support and direction from Professor Wang Xudong of the Palace Museum of China, to whom we are very grateful.

Author contributions

CBL performed the multi-band image analysis, microscopic investigation, and digital reconstruction of the mural and wrote the first draft of this paper. SBM, and SML conceptualized the main research ideas of this work and guided the direction of this study. YZR provided guidance for the pigment analysis. SZW performed the SEM/EDX analyses on the pigment samples. ZJL performed the LC/MS analyses on the pigment samples. SBW performed the XRD analyses on the pigment samples. WZ performed the m-RS analyses on the pigment samples. YYP performed the in situ pXRF analysis of the mural. All of the authors read and approved the final manuscript.

Funding

This study was supported by the National Social Science Foundation of China (Grant Nos. 19EA195), Natural Science Foundation of Gansu Province (Grant No. 20JR5RA055), Key projects of the Joint Fund for regional innovation and development of the National Natural Science Foundation of China (Grant No. U21A20282), Gansu Province Youth Science and Technology Fund (Grant No. 21JR7RA758), the Science and Technology Project of Gansu Province (Grant No. 21JR7RA759), and the111 Project (D18004).

Availability of data and materials

All of the data that were generated or analyzed during the study period are included in this paper.

Declarations

Competing interests

The authors declare no conflict of interest in relation to this publication.

Author details

[1]China-Central Asia "the Belt and Road" Joint Laboratory On Human and Environment Research, Key Laboratory of Cultural Heritage Research and Conservation, School of Culture Heritage, Northwest University, Xi'an 710127, China. [2]School of Culture Heritage, Northwest University, Xi'an 710127, China. [3]Key Laboratory of Cultural Heritage Research and Conservation, Ministry of Education, Xi'an, China. [4]National Research Center for Conservation of Ancient Wall Paintings and Earthen Sites, Gansu Province, Dunhuang Academy, Dunhuang 736200, China.

Received: 10 May 2022 Accepted: 18 September 2022
Published online: 19 October 2022

References

1. Chen H, Chen Q. Making of a digital film interpretation of the Sattva Jataka Tale in Mogao Cave 254. Dunhuang Research. 2014;6:55–60.
2. Martin AE. Bodily transfer and sacrificial gestures: rethinking the Hungry Tigress Jataka in Mogao Cave 254 Department of Art and Art History. Salt Lake: University of Utah; 2014.
3. Pei S, He Y. Study on the importance of protecting the original artistic value of the cultural heritage of the Mogao Grottoes. In: Proceedings of the 4th International Conference on Art Studies: Science, Experience, Education (ICASSEE 2020): conference proceedings. 2020 Aug 27–28. p. 264–68. https://doi.org/10.2991/assehr.k.200907.047
4. Yu S, Wu J, Wang J. Acquisition and processing of the photographic images of the 3D faces inside the narrow caves of the Mogao Grottoes—taking the digitization of the Mogao Cave 254 as an example. Dunhuang Res. 2012;6:108–12.
5. Peitroni E, Ferdani D. Virtual restoration and virtual reconstruction in cultural heritage: terminology, methodologies, visual representation techniques and cognitive models. Information. 2021;12(4):167. https://doi.org/10.3390/info12040167.
6. Costume and Makeup [Internet]. Dunhuang Academy; 2020 [accessed 2022.3.8]. http://public.dha.ac.cn/zhuanti/slmz/sec5/section5-1.html
7. Aswatha SM, Mukherjee J, Bhowmick P. An integrated repainting system for digital restoration of Vijayanagara murals. Int J Image Graph. 2016;16(1):1–28. https://doi.org/10.1142/S0219467816500054.

8. Wang H-L, Han P-H, Chen Y-M, Chen K-W, Lin X, Lee M-S, et al. 2018. Dunhuang Mural restoration using deep learning. In: SA '18: SIGGRAPH Asia 2018: Technical Briefs. Tokyo
9. Stenger J, Khandekar N, Raskar R, Cuellar S, Mohan A, Gschwind RJ. Conservation of a room: a treatment proposal for Mark Rothko's Harvard Murals. Stud Conserv. 2016;61(6):348–61. https://doi.org/10.1179/2047058415Y.0000000010.
10. Wei B, Liu Y, Pan Y. Using hybrid knowledge engineering and image processing in color virtual restoration of ancient murals. IEEE Trans Knowl Data Eng. 2003;15(5):1338–43. https://doi.org/10.1109/TKDE.2003.1232282.
11. Schönlieb C-B. Unveiling the Invisible: mathematical approaches for virtual image restoration in the arts. In: Bridges 2020: Mathematics, Art, Music, Architecture, Education, Culture: conference Proceedings. 2020 Aug 1–5 9–10.
12. Blažek J, Zitová B, Beneš M, Hradilová J. Fresco restoration: Digital image processing approach. In: 17th European Signal Processing Conference (EUSIPCO 2009): Conference proceedings. 2009 Aug 24–28; Glasgow, UK. 1210–14.
13. Original materials and techniques. In: Agnew N, Wong L, editors. The conservation of Cave 85 at the Mogao Grottoes, Dunhuang. USA: Getty Publications; 2013. p. 155–89.
14. Schilling MR, Mazurek J, Carson D, Bomin S, Yuquan F, Zanfeng M. Analytical research in Cave 85. In: Agnew N, editor. Conservation of ancient sites on the silk road: Proceedings of the Second International Conference on the Conservation of Grotto Sites. USA: Getty Publications 2010 438–64.
15. Ogura D, Nakata Y, Hokoi S, Takabayashi H, Okada K, Bomin S, et al. Influence of light environment on deterioration of mural paintings in Mogao Cave 285. Dunhuang. 2019. https://doi.org/10.1063/1.5132732.
16. Guo Q, Staff RA, Lu C, Cheng L, Dee M, Chen Y, et al. A new approach to the chronology of caves 268/272/275 in the Dunhuang Mogao Grottoes: combining radiocarbon dates and archaeological information within a Bayesian statistical framework. Radiocarbon. 2018;60(2):667–79. https://doi.org/10.1017/RDC.2018.4.
17. Xu L, Zhou G, Li Y. 1983. Report on the analysis by X-ray diffraction of inorganic pigments used in murals and color sculptures in Mogao Grottoes. Dunhuang Research. 187–97
18. Li ZX. Pigment analysis on Tang Dynasty murals at the Mogao Grottoes. Dunhuang Research. 2002;74(4):11–7.
19. Nöller R. Cinnabar reviewed: characterization of the red pigment and its reactions. Stud Conserv. 2015;60(2):79–87. https://doi.org/10.1179/2047058413Y.0000000089.
20. Vermeulen M, Sanyova J, Janssens K, Nuyts G, De Meyer S, De Wael K. The darkening of copper-or lead-based pigments explained by a structural modification of natural orpiment: a spectroscopic and electrochemical study. J Anal At Spectrom. 2017;32(7):1331–41. https://doi.org/10.1039/C7JA00047B.
21. Aze S, Vallet J-M, Baronnet A, Grauby O. The fading of miniumite pigment in wall paintings: tracking the physico-chemical transformations by means of complementary microanalysis techniques. Eur J Mineral. 2006;18(6):835–43. https://doi.org/10.1127/0935-1221/2006/0018-0835.
22. Wang W, Ma Y, Ma X, Wu F, Ma X, An L, et al. Diversity and seasonal dynamics of airborne bacteria in the Mogao Grottoes, Dunhuang. China Aerobiologia. 2012;28(1):27–38. https://doi.org/10.1007/s10453-011-9208-0.
23. Imperi F, Caneva G, Cancellieri L, Ricci MA, Sodo A, Visca P. The bacterial etiology of rosy discoloration of ancient wall paintings. Environ Microbiol. 2007;9(11):2894–902. https://doi.org/10.1111/j.1462-2920.2007.01393.x.
24. Vermeulen M, Janssens K, Sanyova J, Rahemi V, McGlinchey C, De Wael K. Assessing the stability of arsenic sulfide pigments and influence of the binder media on their degradation by means of spectroscopic and electrochemical techniques. Microchem J. 2018. https://doi.org/10.1016/j.microc.2018.01.004.
25. Piqué F, Verri G. UV-Induced Fluorescence Photography. In: Organic materials in wall paintings. USA: Getty Conservation Institute; 2015 18–20
26. Pelagotti A, Del Mastio A, De Rosa A, Piva A. Multispectral imaging of paintings. IEEE Signal Process Mag. 2008;25(4):27–36. https://doi.org/10.1109/MSP.2008.923095.
27. Wilson M, France F, Bolser C. Multispectral imaging for scientific analysis and preservation of cultural heritage materials. In:Archiving Conference : Conference Proceedings. 2018 (1):147–50. https://doi.org/10.2352/issn.2168-3204.2018.1.0.32
28. Cosentino A. Practical notes on ultraviolet technical photography for art examination. Conservar Património. 2015;21:53–62.
29. Verri G, Saunders D. Xenon flash for reflectance and luminescence (multispectral) imaging in cultural heritage applications. British Museum Technical Bulletin. 2014;8:83–92.
30. Verri G. The spatially resolved characterization of Egyptian blue Han blue and Han purple by photo-induced luminescence digital imaging. Anal Bioanal Chem. 2009;394(4):1011–21. https://doi.org/10.1007/s00216-009-2693-0.
31. Dyer J, Tamburini D, O'Connell ER, Harrison A. A multispectral imaging approach integrated into the study of late antique textiles from Egypt. PLoS ONE. 2018;13(10): e0204699. https://doi.org/10.1371/journal.pone.0204699.
32. Tamburini D, Dyer J. Fiber optic reflectance spectroscopy and multispectral imaging for the non-invasive investigation of Asian colorants in Chinese textiles from Dunhuang (7th-10th century AD). Dyes Pigm. 2019;162:494–511. https://doi.org/10.1016/j.dyepig.2018.10.054.
33. Colantonio C, Pelosi C, D'Alessandro L, Sottile S, Calabrò G, Melis M. Hypercolorimetric multispectral imaging system for cultural heritage diagnostics: an innovative study for copper painting examination. Eur Phys J Plus. 2018;133(12):1–12. https://doi.org/10.1140/epjp/i2018-12370-9.
34. Cosentino A. Studies Panoramic, macro and micro multispectral imaging: an affordable system for mapping pigments on artworks. J Conserv Mus Stud. 2015;13(1):1–17. https://doi.org/10.5334/jcms.1021224.
35. Webb EK, Summerour R, Giaccai J. A case study using multispectral & hyperspectral imaging for the identification & characterization of materials on archaeological Andean painted textiles. Textile Group Postprints. 2014;24:23–35.
36. Dyer J, Verri G, Cupitt J. Multispectral imaging in reflectance and photo-induced luminscence modes: a user manual. The British Museum. 2013. 1–184
37. Cosentino A. Identification of pigments by multispectral imaging; a flowchart method. Heritage Sci. 2014;2(1):1–12. https://doi.org/10.1186/2050-7445-2-8.
38. Fuster-López L,Marcello P, Stols-Witlox M. UV-Vis Luminescence imaging techniques. Editorial Universitat Politècnica de València; 2020. 47–49
39. de la Rie ER. Fluorescence of paint and varnish layers (part 1). Stud Conserv. 1982;27(1):1–7. https://doi.org/10.1179/sic.1982.27.1.1.
40. Smith GD, Clark RJ. Note on lead(II) oxide in mediaeval frescoes from the monastery of San Baudelio Spain. Appl Spectros. 2002;56(6):804–6. https://doi.org/10.1366/000370202760077577.
41. Zhou Z, Shen L, Li C, Wang N, Chen X, Yang J, et al. Investigation of gilding materials and techniques in wall paintings of Kizil Grottoes. Microchem J. 2020;154:104548. https://doi.org/10.1016/j.microc.2019.104548.
42. Tamburini D, Dyer J, Bonaduce I. The characterization of shellac resin by flow injection and liquid chromatography coupled with electrospray ionization and mass spectrometry. Sci Rep. 2017;7(1):1–15. https://doi.org/10.1038/s41598-017-14907-7.
43. Berbers SVJ, Tamburini D, van Bommel MR, Dyer J. Historical formulations of lake pigments and dyes derived from lac: a study of compositional variability. Dyes Pigm. 2019. https://doi.org/10.1016/j.dyepig.2019.107579.
44. Clementi C, Doherty B, Gentili PL, Miliani C, Romani A, Brunetti BG, et al. Vibrational and electronic properties of painting lakes. Appl Phys A. 2008;92(1):25–33. https://doi.org/10.1007/s00339-008-4474-6.
45. Tamburini D. Investigating Asian colorants in Chinese textiles from Dunhuang (7th-10th century AD) by high performance liquid chromatography tandem mass spectrometry–towards the creation of a mass spectra database. Dyes Pigm. 2019;163:454–74. https://doi.org/10.1016/j.dyepig.2018.12.025.
46. Nabais P, Melo MJ, Lopes JA, Vieira M, Castro R, Romani A. Organic colorants based on lac dye and brazilwood as markers for a chronology and geography of medieval scriptoria: a chemometrics approach. Heritage Sci. 2021;9(1):1–18. https://doi.org/10.1186/s40494-021-00490-8.
47. Vermeulen M, Nuyts G, Sanyova J, Vila A, Buti D, Suuronen JP, et al. Visualization of As(III) and As(V) distributions in degraded paint

micro-samples from Baroque-and Rococo-era paintings. J Anal At Spectrom. 2016;31(9):1913–21. https://doi.org/10.1039/C6JA00134C.
48. Vanmeert F, de Keyser N, van Loon A, Klaassen L, Noble P, Janssens K. Transmission and reflection mode macroscopic X-ray powder diffraction imaging for the noninvasive visualization of paint degradation in still life paintings by Jan Davidsz de Heem. Anal Chem. 2019;91(11):7153–61. https://doi.org/10.1021/acs.analchem.9b00328.
49. Gebremariam KF, Kvittingen L, Banica F-G. Physico-chemical characterization of pigments and binders of murals in a church in Ethiopia. Archaeometry. 2016;58(2):271–83. https://doi.org/10.1111/arcm.12163.
50. Lama E, Prieto-Taboada N, Etxebarria I, Bermejo J, Castro K, Arana G, et al. Spectroscopic characterization of xx century mural paintings of punta begoña's galleries under conservation works. Microchem J. 2021;168:106423. https://doi.org/10.1016/j.microc.2021.106423.
51. Rosenzweig A, Finney JJ. The unit cell of carminite. Am Mineral. 1959;44(5–6):663–5.
52. Mazzoleni P, Barone G, Raneri S, Aquilia E, Bersani D, Cirrincione R. Application of micro-Raman spectroscopy for the identification of unclassified minerals preserved in old museum collections. Pliniu. 2016;42:112–24.
53. Yi L, Laren L. Preliminary study of the characteristics and genesis of arsenate minerals in the oxidized zone of the Debao skarn-type Cu-Sn ore deposit in Guangxi. Acta Geologica Sinica-English Edition. 1991;4(2):187–94. https://doi.org/10.1111/j.1755-6724.1991.mp4002006.x.
54. Wang LQ, Ma YN, Zhang YX, Zhao X, He QJ, Guo JY, et al. Pigment identification of Sleeping Buddha at World Cultural Heritage Dazu Rock Carvings with mu-Raman spectroscopy and related research. Spectrosc Spectral Anal. 2020;40:3199–204. https://doi.org/10.3964/j.issn.1000-0593(2020)10-3199-06.
55. Taylor MR, Bevan DJM, Pring A. The crystal structure of carminite: refinement and bond valence calculations. Mineral Mag. 1996;60(402):805–11. https://doi.org/10.1180/minmag.1996.060.402.11.
56. Foshag WF. Carminite and associated minerals from Mapimi. Mexico Am Mineral. 1937;22(5):479–84.
57. Chander S. Oxidation/reduction effects in depression of sulfide minerals—a review. Mining Metall Explor. 1985;2(1):26–35. https://doi.org/10.1007/BF03402591.
58. Corbeil MC, Helwig K. An occurrence of pararealgar as an original or altered artists' pigment. Stud Conserv. 1995;40(2):133–8. https://doi.org/10.1179/sic.1995.40.2.133.
59. Zhang Y, Wang J, Liu H. Integrated analysis of pigments on murals and sculptures in Mogao Grottoes. Anal Lett. 2015;48(15):2400–13. https://doi.org/10.1080/00032719.2015.1038557.
60. Coccato A, Moens L, Vandenabeele P. On the stability of mediaeval inorganic pigments: a literature review of the effect of climate, material selection, biological activity, analysis and conservation treatments. Heritage Sci. 2017;5(1):1–25. https://doi.org/10.1186/s40494-017-0125-6.

Publisher's Note

Springer Nature remains neutral with regard to jurisdictional claims in published maps and institutional affiliations.

Submit your manuscript to a SpringerOpen journal and benefit from:

- ► Convenient online submission
- ► Rigorous peer review
- ► Open access: articles freely available online
- ► High visibility within the field
- ► Retaining the copyright to your article

Submit your next manuscript at ► springeropen.com